Published October 31, 2016

pMHC affinity controls duration of CD8$^+$ T cell–DC interactions and imprints timing of effector differentiation versus expansion

Aleksandra J. Ozga,[1] Federica Moalli,[1]* Jun Abe,[1]* Jim Swoger,[2,3] James Sharpe,[2,3,4] Dietmar Zehn,[5,6] Mario Kreutzfeldt,[7] Doron Merkler,[7] Jorge Ripoll,[8,9] and Jens V. Stein[1]

[1]Theodor Kocher Institute, University of Bern, 3012 Bern, Switzerland
[2]Systems Biology Research Unit, European Molecular Biology Laboratory/Centre for Genomic Regulation, Barcelona Institute of Science and Technology, 08003 Barcelona, Spain
[3]Universitat Pompeu Fabra, 08002 Barcelona, Spain
[4]Institució Catalana de Recerca i Estudis Avançats, 08010 Barcelona, Spain
[5]Swiss Vaccine Research Institute, Centre des laboratoires d'Epalinges, 1066 Epalinges, Switzerland
[6]Division of Immunology and Allergy, Department of Medicine, Lausanne University Hospital, 1011 Lausanne, Switzerland
[7]Department of Pathology and Immunology, University of Geneva, 1211 Geneva, Switzerland
[8]Department of Bioengineering and Aerospace Engineering, Universidad Carlos III of Madrid, 28911 Madrid, Spain
[9]Experimental Medicine and Surgery Unit, Instituto de Investigación Sanitaria del Hospital Gregorio Marañón, 28007 Madrid, Spain

During adaptive immune responses, CD8$^+$ T cells with low TCR affinities are released early into the circulation before high-affinity clones become dominant at later time points. How functional avidity maturation is orchestrated in lymphoid tissue and how low-affinity cells contribute to host protection remains unclear. In this study, we used intravital imaging of reactive lymph nodes (LNs) to show that T cells rapidly attached to dendritic cells irrespective of TCR affinity, whereas one day later, the duration of these stable interactions ceased progressively with lowering peptide major histocompatibility complex (pMHC) affinity. This correlated inversely BATF (basic leucine zipper transcription factor, ATF-like) and IRF4 (interferon-regulated factor 4) induction and timing of effector differentiation, as low affinity–primed T cells acquired cytotoxic activity earlier than high affinity–primed ones. After activation, low-affinity effector CD8$^+$ T cells accumulated at efferent lymphatic vessels for egress, whereas high affinity–stimulated CD8$^+$ T cells moved to interfollicular regions in a CXCR3-dependent manner for sustained pMHC stimulation and prolonged expansion. The early release of low-affinity effector T cells led to rapid target cell elimination outside reactive LNs. Our data provide a model for affinity-dependent spatiotemporal orchestration of CD8$^+$ T cell activation inside LNs leading to functional avidity maturation and uncover a role for low-affinity effector T cells during early microbial containment.

INTRODUCTION

CD8$^+$ T cells recognize pathogen-derived peptides presented by MHC on DCs that have migrated from the site of infection to the T cell area of secondary lymphoid organs (SLOs), including LNs. Both high- and low-affinity TCR–pMHC interactions drive CD8$^+$ T cell proliferation and effector/memory cell formation, and the breadth of recruited TCR affinities is associated with improved host protection (Zehn et al., 2009; van Gisbergen et al., 2011). Strikingly, the functional avidity of T cell responses, which encompasses preferential expansion of high-affinity T cell clones and optimization of the signal transduction machinery (Slifka and Whitton, 2001), improves over the course of an immune response (Busch and Pamer, 1999; Savage et al., 1999; Zehn et al., 2009). Thus, effector CD8$^+$ T cells with low affinity for pMHC rejoin the circulation earlier than high-affinity clones, which proliferate longer in SLOs. This maturation of pMHC-specific CD8$^+$ T cell responses occurs at the population level, evolving from a pool of cells with diverse TCR affinities for pMHCs being recruited and activated inside SLOs (Horwitz et al., 1994; Turner et al., 2006). A recent study using highly sensitive dodecamer labeling has uncovered an unexpected abundance of low-affinity CD8$^+$ T cells, often outnumbering high-affinity

*F. Moalli and J. Abe contributed equally to this paper.

Correspondence to Jens V. Stein: jstein@tki.unibe.ch

D. Zehn's present address is Physiology Weihenstephan, Technische Universität München, 85354 Freising, Germany.

Abbreviations used: 2PM, two-photon microscopy; 3D, three-dimensional; APL, altered peptide ligand; FDC, follicular dendritic cell; FOV, field of view; FSC, forward scatter; HEV, high endothelial venule; IFR, interfollicular region; LCMV-OVA, OVA-expressing lymphocytic choriomeningitis virus; MFI, median fluorescence intensity; PFA, paraformaldehyde; p.i., postinfection; qPCR, quantitative PCR; SLO, secondary lymphoid organ; SPIM, selective plane illumination microscopy.

The Rockefeller University Press $30.00
J. Exp. Med. 2016
https://doi.org/10.1084/jem.20160206

Published October 31, 2016

clones by an order of magnitude (Huang et al., 2016). Yet, how TCR affinity regulates T cell–DC interactions that imprint $CD8^+$ T cell activation, expansion, and differentiation within lymphoid tissue has not been well studied. Similarly, the role of the early wave of released low-affinity effector T cells remains unclear.

Intravital two-photon microscopy (2PM) studies have identified three phases of interactions between T cells and DCs: in phase 1 (lasting from 0–8 h after T cell entry into LNs), continuously migrating $CD8^+$ T cells sample DCs presenting cognate pMHC. During this sampling, they gradually up-regulate early activation markers such as CD69 and integrate signals to pass an activation threshold that permits them to stably interact with DCs (phase 2; here, stable interactions are defined as lasting >30 min, the duration of a typical 2PM image sequence). The kinetics of the phase 1 to phase 2 transition critically depend on cognate pMHC levels on DCs. When cognate pMHC levels are high, $CD8^+$ T cells almost immediately engage in phase 2–type interactions with DCs, whereas very low pMHC levels prevent lasting T cell engagement with DCs (Mempel et al., 2004; Germain et al., 2006; Henrickson et al., 2008, 2013). Stable interactions last approximately from 8 to 20 h after T cell entry into LNs and are critical for optimal T cell activation (Iezzi et al., 1998). Yet, the precise duration and its regulation by TCR affinity have not been investigated in detail (Moreau et al., 2012; Pace et al., 2012). In phase 3 (>20 h after T cell entry), $CD8^+$ T cells detach from DCs, resume their motility, and begin to divide inside LNs before egressing via efferent lymphatic vessels in a sphingosine-1–phosphate receptor 1 (S1P1)–dependent manner (Schwab and Cyster, 2007). The behavior of dividing high- and low-affinity $CD8^+$ T cell clones in the time window between DC detachment and egress is not well understood. Thus, it is controversial whether daughter $CD8^+$ T cells retain the capacity of interacting with pMHC-presenting DCs. Although a short TCR stimulus suffices to induce a $CD8^+$ T cell division program without further stimulation (Kaech and Ahmed, 2001; van Stipdonk et al., 2001), prolonged antigen exposure increases the magnitude of $CD8^+$ T cell expansion (Curtsinger et al., 2003; van Stipdonk et al., 2003; Prlic et al., 2006). Similarly, the kinetics of $CD8^+$ T cell effector function acquisition, i.e., cytotoxic activity, and its relation with TCR affinity after DC priming have not been investigated in vivo. Recent studies have shown that $CD8^+$ T cell expansion requires the expression of the basic leucine zipper transcription factor, ATF-like (BATF) and interferon-regulated factor 4 (IRF4). BATF promotes expression of proliferation-related genes and represses genes involved in effector function including granzyme B (*Gzmb*; Kurachi et al., 2014), whereas its cooperative binding factor IRF4 is induced in a TCR affinity–dependent manner (Man et al., 2013; Murphy et al., 2013; Yao et al., 2013; Nayar et al., 2014).

To analyze the impact of TCR–pMHC affinity on T cell–DC interaction patterns, we used 2PM imaging of reactive LNs in combination with a well-defined TCR transgenic T cell transfer system (Kearney et al., 1994) and a set of altered peptide ligands (APLs). We report comparable digital onset of stable T cell–DC interactions irrespective of affinity, whereas the overall duration of stable T cell–DC interactions was controlled by TCR affinity in an analog manner and imprinted the timing of effector differentiation. Whole-LN reconstructions uncovered that intranodal positioning of expanding daughter cells was critically influenced by TCR–pMHC affinity and determined their capacity to either engage in CXCR3-dependent successive $pMHC^+$ DC encounters or to rapidly egress for early containment of local viral spread. In sum, our data model the functional avidity maturation characteristic of T cell responses.

RESULTS

TCR–pMHC affinity controls the duration of stable $CD8^+$ T cell–DC interactions

We first analyzed the influence of pMHC affinity on T cell deceleration upon DC encounter (phase 1 to 2 transition), as well as on detachment from DCs that precedes cell division (phase 2 to phase 3 transition). DCs were either loaded with high-affinity OVA-derived peptide-SIINFEKL (N4), APL SII QFEKL (Q4), or SIITFEKL (T4), each at 100 nM and injected s.c. to activate OT-I T cells in draining LNs. Although all peptides bind equally well to $H\text{-}2K^b$ (Zehn et al., 2009; Moreau et al., 2012), they induce quantitatively distinct expansion of OT-I T cells, with N4 stimulation leading to the highest OT-I expansion, Q4 to intermediate, and T4 to low but still detectable levels. The peptide pulsing concentration was chosen because it induces maximal activation of T4-stimulated thymocytes (Daniels et al., 2006) and OT-I T cells (not depicted). 3 h after OT-I T cell transfer, their LN dwell time was synchronized by blocking further homing with an anti-CD62L mAb (Mempel et al., 2004). At specified times, we performed 2PM of reactive popliteal LNs to quantify the effect of pMHC affinity on initial T cell–DC interactions in vivo (Fig. 1 A). In our experimental system, the majority of OT-I T cells slowed down and stably interacted with DCs during the initial 2–10 h after T cell transfer, irrespective of pMHC affinity (88 vs. 84 vs. 76% stable interactions with N4-, Q4-, and T4-pulsed DCs, respectively; Fig. 1, B–D; and Videos 1–3), although we observed a small but significant inverse correlation between stable T cell adhesion and pMHC affinity (Fig. 1 D), as described previously (Moreau et al., 2012). At 24–32 h after T cell transfer, most T4-primed OT-I T cells resumed their motility, resulting in few long-term DC interactions and increased speeds (16% stable interactions; Fig. 1, B–D; and Video 6). In contrast, 47% of OT-I T cell interactions with Q4-pulsed and almost 60% of interactions with N4-pulsed DCs remained stable during this late phase (Fig. 1, B–D; and Videos 4 and 5). Accordingly, N4-primed OT-I T cell speeds were persistently low throughout the first 32 h after transfer (Fig. 1 C).

To corroborate our observations in a separate system, we cotransferred two T cell populations with distinct affin-

Published October 31, 2016

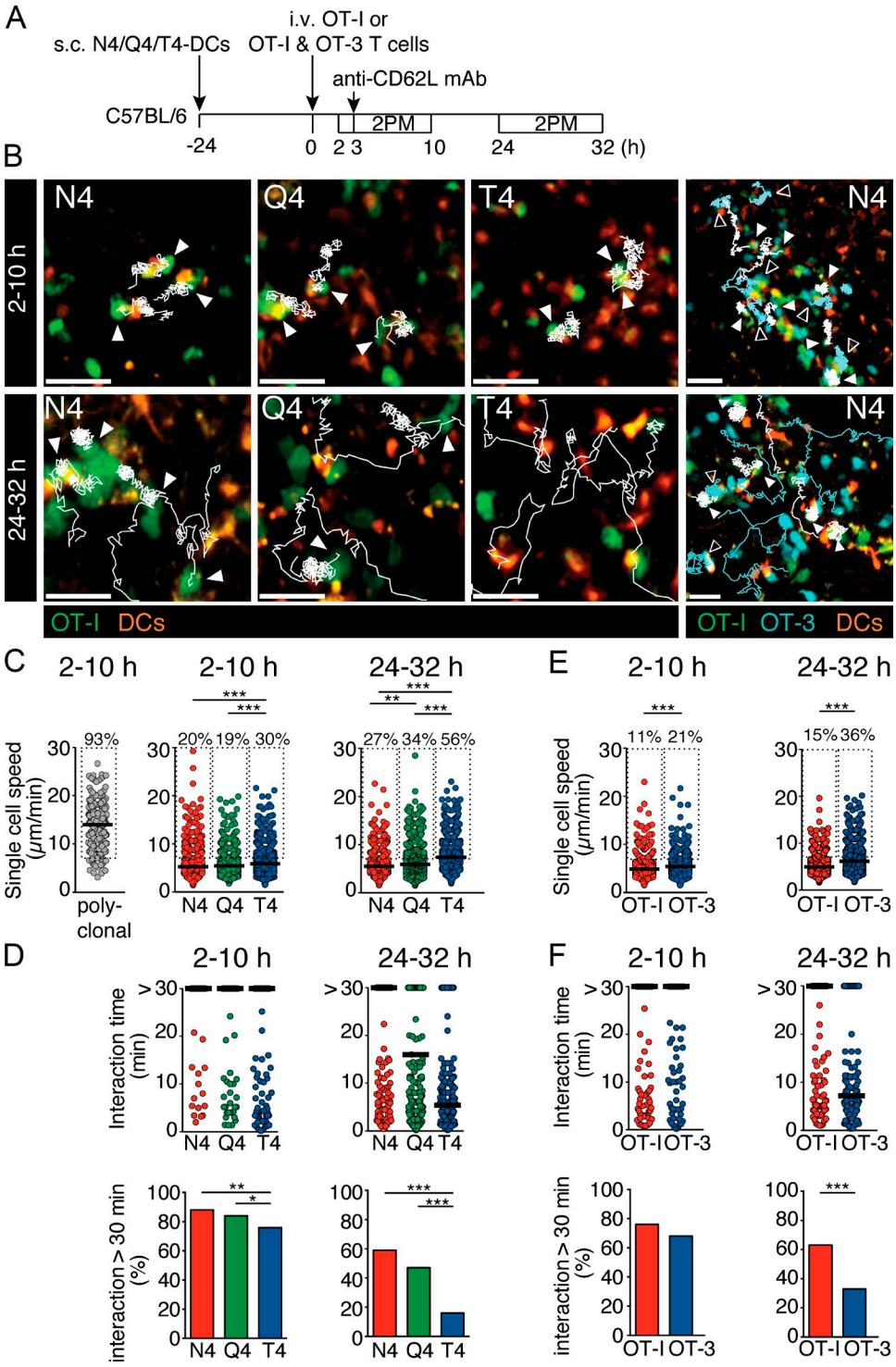

Figure 1. **TCR affinity controls duration of stable CD8⁺ T cell–DC interactions in vivo.** (A) Experimental layout. T cell–DC interactions in popliteal LNs were analyzed by 2PM in the presence of s.c. peptide-pulsed DCs at the indicated time points after i.v. T cell transfer. (B) Representative 2PM images of OT-I T cell tracks (white lines) or OT-3 T cell tracks (blue lines) in the presence of peptide-pulsed DCs at early (2–10 h) or late (24–32 h) time points after T cell transfer. Arrowheads point to stable (>30 min) OT-I T cell–DC (closed) or OT-3 T cell–DC (open) interactions. Bar, 20 µm. (C and E) Single-T cell speeds at each time point. Polyclonal T cell speeds are included for comparison. Percentages refer to tracks in dashed-line boxes showing single-cell speeds of >7

Published October 31, 2016

ities for a given pMHC for side-by-side comparison. OT-3 $CD8^+$ T cells carry a TCR with 50-fold decreased functional avidity for the N4 peptide as compared with OT-I T cells (Enouz et al., 2012). We performed 2PM experiments after adoptive transfer of N4-pulsed DCs, followed by cotransfer of OT-I and OT-3 T cells (Fig. 1 A). During the first 2–10 h after T cell transfer, OT-3 T cells reduced their speeds to levels comparable with OT-I T cells and efficiently formed stable contacts with DCs (76 vs. 68% for OT-I and OT-3 cells, respectively; Fig. 1, B, E, and F; and Video 7). At 24–32 h after transfer, OT-3 T cells had regained their motility and detached from N4-pulsed DCs, in contrast to OT-I T cells (63 vs. 33% stably interacting OT-I and OT-3 T cells, respectively; Fig. 1, B, E, and F; and Video 8). To control for potential interaction artifacts introduced by the high number of cotransferred OT-I and OT-3 T cells, we lowered the amount of transferred T cells to 0.5×10^6 cells each, the lowest possible number that allowed us to detect sufficient interactions in vivo. Similar to our observations using high numbers of transferred T cells, we found that the percentage of stable interactions was significantly reduced for OT-3 T cells 24 h after transfer as compared with OT-I T cells (85 vs. 21% stably interacting OT-I and OT-3 T cells, respectively). Collectively, our intravital imaging data suggest that $CD8^+$ T cell deceleration (i.e., phase 1 to 2 transition) rapidly occurred irrespective of pMHC affinity and led to the formation of stable contacts with DCs. However, the overall duration of these stable interactions (i.e., phase 2 to 3 transition) was controlled by pMHC affinity in our experimental system.

pMHC affinity inversely correlates with timing of effector differentiation

High-, medium-, and low-affinity pMHC-primed $CD8^+$ T cells participate in immune responses. Yet, how affinity controls timing of effector function acquisition has not been comprehensively investigated in vivo. We sorted N4-, Q4-, or T4-stimulated OT-I T cells 60 h after transfer and performed real-time quantitative PCR (qPCR) of gene expression involved in effector differentiation and proliferation. The transcriptional factors BATF and IRF4 act as checkpoints in $CD8^+$ T cell differentiation by restraining expression of effector genes until a critical threshold of activation has been reached (Man et al., 2013; Kurachi et al., 2014). We observed increased induction of *Batf* and *Irf4* mRNA in N4-primed OT-I T cells, whereas Q4- and T4-primed OT-I T cells showed reduced levels that inversely correlated with pMHC affinity (Fig. 2 A). In contrast, OT-I T cells primed with low-affinity peptides (Q4 and T4) expressed significantly higher levels of the cytotoxic effector gene *GzmB* and to a lesser extent perforin 1 (*Prf1*) mRNA than N4-stimulated OT-I T cells (Fig. 2 A). We confirmed increased GzmB expression in low affinity–primed OT-I T cells by flow cytometry both in the percentage of positive cells and their median fluorescence intensity (MFI; Fig. 2 B). The lower expression of effector molecules in high affinity–primed T cells was transient, as 108 h after transfer, LN-resident N4-stimulated OT-I T cells expressed comparable levels of GzmB and Prf1 as T4-stimulated OT-I T cells at the 60-h time point (Fig. 2 C). Thus, the shortened duration of stable interactions with DCs correlated with early expression of cytotoxic genes in low and medium TCR affinity–primed OT-I T cells. We obtained similar results when we compared GzmB expression and normalized MFI in N4-pulsed DC-stimulated OT-I versus OT-3 T cells 60 h after T cell transfer ($16.9 \pm 5.2\%$ and $32.6 \pm 9.7\%$ $GzmB^+$ OT-I and OT-3 T cells, respectively, $P < 0.001$; 135 ± 36 normalized MFI of *GzmB* mRNA levels expression in OT-3 compared with OT-I levels, $P < 0.01$; all values are mean $\pm$ SD).

GzmB and Prf1 are critical components of the killing machinery of cytotoxic $CD8^+$ T cells (Cullen and Martin, 2008). We asked whether increased effector gene expression by OT-I T cells primed with APLs correlated with an accelerated acquisition of cytotoxic activity. We focused on the ability to eliminate newly arriving unpulsed and N4-, Q4-, or T4-pulsed DCs injected 60 or 84 h (2.5 or 3.5 d) after OT-I T cell transfer. We used *Prf1*-deficient mice as hosts to avoid endogenous T cell–mediated cytotoxicity. 24 h after DC transfer, we compared ratios of unpulsed DCs to N4-, Q4-, or T4-pulsed DCs (Fig. 2 D). Control experiments showed that peptide pulsing did not affect DC recovery in the absence of effector $CD8^+$ T cells (not depicted). At both 84 and 108 h after transfer, we recovered significantly fewer peptide-pulsed DCs in Q4-primed LNs as compared with N4-primed LNs, whereas recovery of peptide-pulsed DCs from T4-primed LNs was similar to N4-primed LNs (Figs. 2, E and F). Because N4 priming induced greater expansion of OT-I T cells than Q4 or T4 priming LNs 84 and 108 h after T cell transfer (Fig. 4 B and not depicted), we normalized DC ratios to OT-I T cell percentages in reactive LNs to calculate their per-cell killing efficacy. Relative to N4-primed OT-I T cells in 84-h–reactive LNs (normalized ratio 1), pulsed DCs were much more efficiently eliminated in reactive LNs containing Q4-primed (normalized ratio 2.5 ± 0.4; mean $\pm$ SEM) and in particular T4-primed OT-I T cells (normalized ratio 5.4 ± 0.7; Fig. 2 G). This trend was maintained 108 h after T cell transfer, as Q4- and T4-primed OT-I T cells eliminated pulsed DCs (normalized ratios 16.9 ± 4.8 and 8.1 ± 1.1, respectively), whereas N4-primed OT-I T cells were the least efficient in DC killing on a per-cell basis at this time point (normalized ratio 0.7 ± 0.2; Fig. 2 G). Thus, although N4-primed OT-I T cells outnumbered Q4- and T4-primed

μm/min. (D and F) T cell–DC interaction times. Each dot represents a single track (C and E) or interaction (D and F). Bars indicate mean (C and E) or median (D and F). (C–F) Data are pooled from at least two independent experiments with four or more mice/eight image sequences per condition and time point. Statistical significance was analyzed for entire datasets by Kruskal-Wallis tests with Dunn's posttest. *, $P < 0.05$; **, $P < 0.01$; ***, $P < 0.001$.

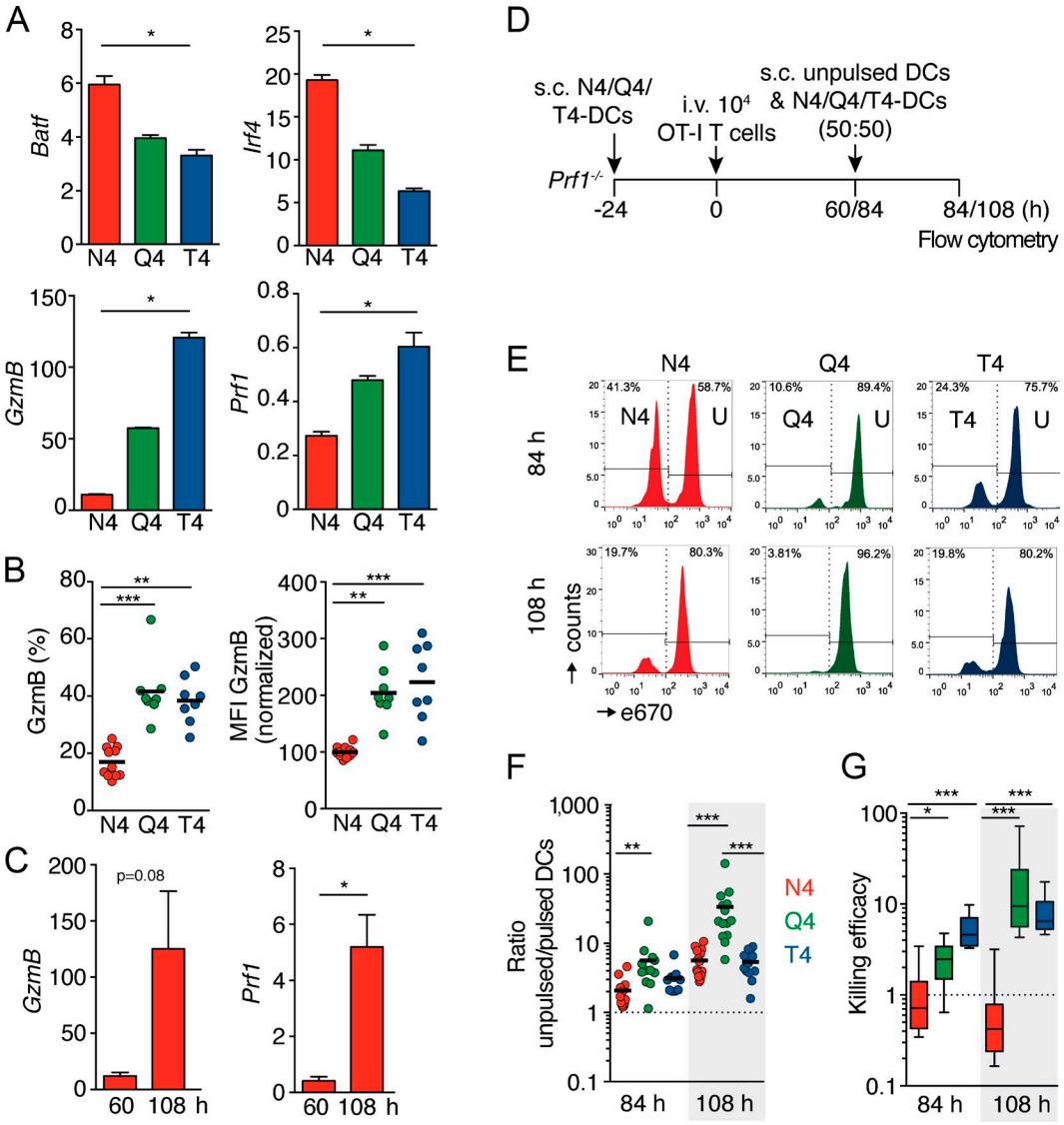

Figure 2. **TCR affinity inversely correlates with onset of effector gene expression and cytotoxic activity in vivo.** (A) mRNA levels of *Batf*, *Irf4*, *Gzmb*, and *Prf1* in divided (e670^{low}) GFP^{+} OT-I T cells sorted 60 h after transfer into recipient mice that contained N4-, Q4-, or T4-pulsed DCs. Relative mRNA levels were normalized to naive OT-I T cell mRNA levels (set to 1). Fold-changes in mRNA levels are shown as mean ± SEM. Data are representative of two independent experiments with RNA from LNs pooled from two to three mice per condition. (B) Flow cytometry of gzmB-positive OT-I T cells and gzmB MFI 60 h after T cell transfer. Each dot represents data from one mouse. Data are pooled from three independent experiments with a total of 8–11 mice per group. (C) Relative mRNA levels of *GzmB* and *Prf1* in N4-stimulated OT-I T cells at 60 h (as in A) and 108 h after transfer. Data are of one experiment with RNA pooled from LNs of two to three mice per condition. Error bars represent mean ± SEM. (D) Experimental layout of DC elimination assay. (E) Flow cytometry plots gated on CD45.1^{+} DCs injected 1 d before into mice that contained activated OT-I T cells (readout at 84 and 108 h after OT-I T cell transfer). e670^{low} DCs were pulsed with peptides, and e670^{high} unpulsed DCs (U) were cotransferred as controls. Data are representative of six independent experiments. (F) Ratio of unpulsed DCs to N4-, Q4-, or T4-pulsed DCs recovered from LNs 84 or 108 h after OT-I T cell transfer. Bars show the mean, with each dot representing a single LN. (G) Killing efficacy as assessed by dividing data in F by the percentage of OT-I T cells in reactive LNs. Calculated values were normalized to the N4/DC ratio divided by the 84-h OT-I T cell percentage. The box extends from the 25th to 75th percentile with the median; whiskers indicate upper and lower range. (F and G) Data are pooled from six independent experiments with total of seven mice per condition. Data were analyzed using Kruskal-Wallis tests with Dunn's posttest (A, B, F, and G) or Student's *t* test (C). *, P < 0.05; **, P < 0.01; ***, P < 0.001.

OT-I T cells by a factor of 10–20 on day 4.5 postinfection (p.i.), these cells did not effectively eliminate target cells on a population level. In vitro killing assays using N4- and APL-primed OT-I cells confirmed that the superior early cytotoxic activity of APL-primed OT-I T cells was not linked to whether target cells presented APL or N4 peptide (not depicted).

Because DC elimination also takes place at the site of s.c. injection (Hermans et al., 2000), we administered an-

Published October 31, 2016

ti-CD62L mAb and the functional S1P1 antagonist FTY720 into immunized mice, effectively locking lymphocytes into reactive LNs. Blockage of migration to the periphery did not lead to significant reduction in pMHC-restricted DC killing in draining LNs (not depicted). Collectively, low affinity–primed T cells show accelerated acquisition of cytotoxic activity inside lymphoid tissue as compared with high affinity–primed T cells.

pMHC affinity regulates CXCR3 expression and global intranodal positioning of activated CD8$^+$ T cells

Because low-affinity CD8$^+$ T cells rejoin the circulation faster than high-affinity pMHC-primed CD8$^+$ T cells (Zehn et al., 2009), we isolated OT-I T cells 60 h after transfer into mice containing N4-, Q4-, or T4-pulsed DCs and analyzed expression of receptors that direct positioning of activated lymphocytes inside reactive LNs. CCR7 and CD62L levels were decreased in all three cell populations to a comparable extent (not depicted). Irrespective of pMHC affinity, activated OT-I T cells showed decreased transcription of *S1P1* mRNA as compared with naive T cells, which is critical for the sequestration of activated T cells inside SLOs (Pham et al., 2008). However, Q4- and T4-stimulated OT-I T cells showed higher levels of *S1pr1* mRNA as compared with N4-primed OT-I T cells (Fig. 3 A). Q4- and T4-primed OT-I T cells also had lower percentages of CD69$^+$ cells than N4-primed OT-I T cells, consistent with a higher propensity of low affinity–stimulated CD8$^+$ T cells to leave lymphoid tissue early after expansion (Fig. 3 B). In contrast, mRNA levels of the proinflammatory chemokine receptor CXCR3 were highest in N4-primed OT-I T cells 60 h after transfer and gradually decreased with lowering pMHC affinity (not depicted). These results were confirmed by flow cytometry analysis of 72- and 96-h (day 3 and 4)–expanded OT-I T cells, both in terms of percentage of CXCR3$^+$ OT-I T cells and of the MFI of positive cells (Fig. 3, C–E). In consequence, Q4- and in particular T4-primed OT-I T cells were impaired in their ability to migrate toward the CXCR3 ligands CXCL9 and, to a lesser extent, CXCL10 in in vitro migration assays as compared with N4-primed OT-I T cells (Fig. 3 F). Similar results were obtained when we compared CD69 and CXCR3 expression patterns in N4-primed OT-I versus OT-3 T cells. At 60 h after T cell transfer, the percentage of CD69 was reduced from 34.6 ± 18.1% for OT-I T cells to 13.7 ± 10.6% ($P < 0.001$) on OT-3 T cells. Although both populations showed similar percentages of CXCR3$^+$ cells, the normalized MFI on OT-3 T cells was reduced by 26.5% ($P < 0.05$) as compared with OT-I T cells.

During inflammation, the CXCR3 ligands CXCL9 and CXCL10 are induced in interfollicular regions (IFRs) and medulla of reactive LNs (Groom et al., 2012; Sung et al., 2012; Kastenmüller et al., 2013). We examined how the CXCR3 expression pattern in N4-, Q4-, or T4-primed OT-I T cells affected their intranodal localization. After adoptive transfer of 10^4 GFP-expressing OT-I T cells into mice containing N4-, Q4-, or T4-pulsed DCs, we isolated reactive LNs on day 1 and 3 after T cell transfer and performed quantitative selective plane illumination microscopy (SPIM) analysis to determine global T cell positioning inside entire LNs (Fig. S1; Abe et al., 2016). Reconstruction of three-dimensional (3D) datasets revealed that 24 h after T cell transfer, OT-I T cells (~260 cells/LN) were located in the T cell zone (Fig. 4 A). At 84 h after T cell transfer, N4- and Q4-primed OT-I cells had massively expanded from the starting population, whereas T4-primed OT-I T cells showed lower expansion (Fig. 4, A and B). Furthermore, the progeny of N4-, Q4-, and T4-primed OT-I T cells showed apparently different intranodal localization patterns, with an affinity-dependent skewing toward cortical or medullary regions (Fig. 4 A). To quantify our observations, we developed a protocol to assess organ-wide OT-I T cell distribution patterns in LN medulla or cortex, further subdividing the cortex into central T cell zone and distal IFRs (Fig. 4 C and Fig. S1). Our analysis revealed that a large proportion of N4-primed OT-I cells remained sequestered inside the T cell zone or efficiently relocalized toward IFRs, whereas fewer Q4- or T4-primed OT-I T cells were detected in the cortex including the T cell zone and IFRs (Fig. 4 D and Videos 9–11). Instead, we found low-affinity daughter cells redistributing to the LN medulla where efferent lymphatic vessels are located (Fig. 4, D and E; and Videos 10 and 11). Consistent with the notion that medullary localization of T4- and Q4-primed OT-I T cells correlates with earlier egress, treatment with the functional S1P1 antagonist FTY720 24 h after T cell transfer increased total numbers OT-I T cells in day 4–reactive LNs under Q4- and T4-priming conditions but had no effect on N4-stimulated OT-I T cell numbers (not depicted).

Successive encounters with pMHC-presenting DCs lead to increased expansion of high affinity–primed CD8$^+$ T cells

The observation that N4-primed OT-I T cell progeny delayed the acquisition of cytotoxic effector function and efficiently redistributed to outer regions of reactive LNs prompted us to investigate whether these cells could interact with incoming DCs. 2PM experiments showed that N4-primed OT-I effector cells were indeed dynamically scanning N4-pulsed DCs transferred 60 h later. In contrast to the primary interactions of naive OT-I T cells, successive interactions of N4-primed daughter cells with N4-pulsed DCs were mostly of short duration, with ~30% of observed encounters lasting >30 min (not depicted). We also observed transient interactions of Q4- and T4-primed OT-I T cells with late-arriving Q4- or T4-pulsed DCs. However, Q4- and T4-pulsed DCs exhibited an apoptotic phenotype, characterized by strong autofluorescence, blebbing, and loss of dendritic-like cell shape in line with flow cytometry data shown in Fig. 2 E. These data support the notion that high affinity–primed T cells retain the capability of interacting with antigen-bearing DCs after initial phase 2–like stable interactions.

To assess the impact of sustained DC encounters, we compared the percentage of OT-I T cells recovered from day

Published October 31, 2016

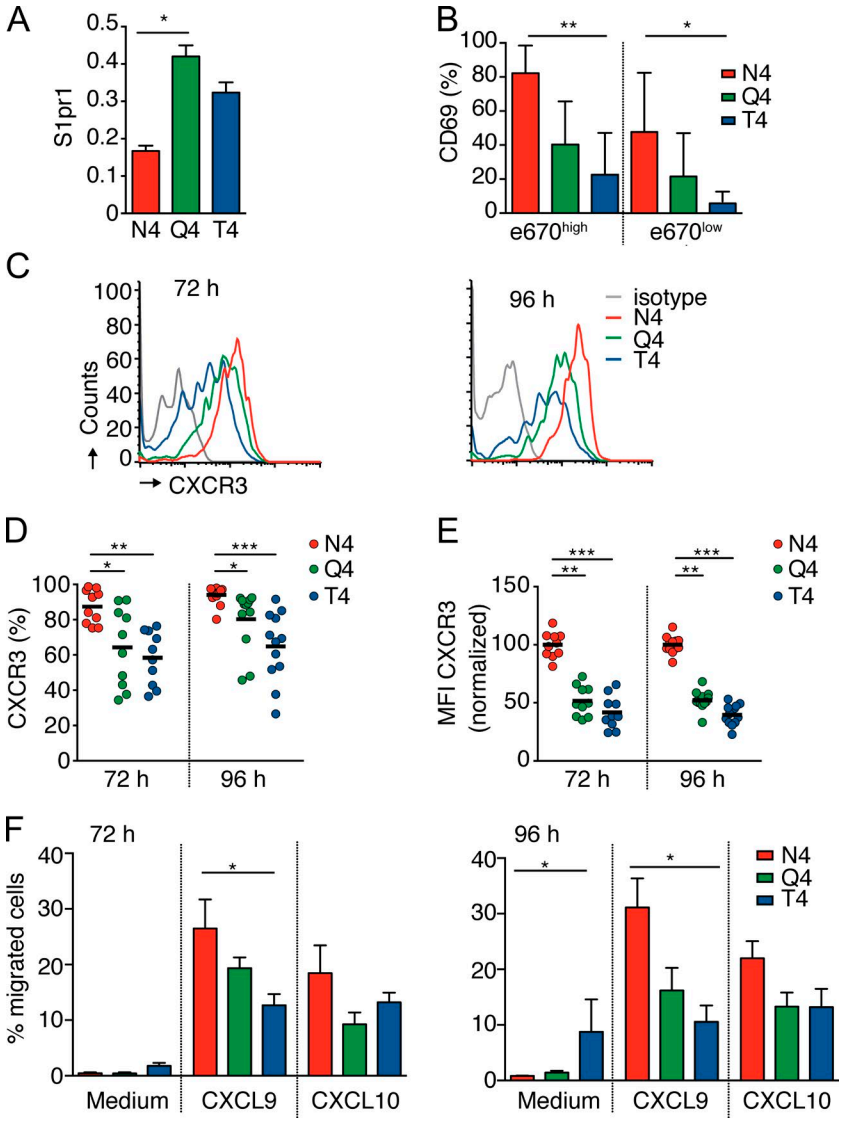

Figure 3. **TCR affinity determines S1P1, CD69, and CXCR3 expression levels on OT-I T cells.** (A and B) mRNA levels of *S1pr1* and CD69 expression in e670-labeled GFP$^+$ OT-I T cells 60 h after transfer into recipient C57BL/6 mice that contained N4-, Q4-, or T4-pulsed DCs. Divided OT-I T cells (e670^{low}) were sorted by flow cytometry and analyzed for relative mRNA levels of *S1pr1* by RT-qPCR as in Fig. 2 A (A) or stained for CD69 expression on divided and undivided OT-I T cells (B; mean ± SD). (A) Data are representative of two independent experiments with RNA from LNs pooled from two to three mice per condition. (B) Data are pooled from three independent experiments with total of five to six mice per condition. (C–E) OT-I T cells were analyzed for CXCR3 expression by flow cytometry 72 and 96 h after transfer in C57BL/6 mice that contained N4-, Q4-, or T4-pulsed DCs. (C) Representative flow cytometry plots of CXCR3 expression. Data are representative of at least five independent experiments. (D) Percentage of CXCR3$^+$ OT-I T cells. Bars indicate the mean. (E) CXCR3 MFI normalized to CXCR3$^+$ N4-primed OT-I T cells. (D and E) Data are pooled from five to six independent experiments with a total of 10–12 mice. (F) In vitro OT-I T cell migration to CXCL9 and CXCL10 at 72 and 96 h after transfer (mean ± SEM). Data are pooled from two independent experiments with total of four mice per condition. Statistical significance was analyzed by Kruskal-Wallis tests with Dunn's posttest. *, $P < 0.05$; **, $P < 0.01$; ***, $P < 0.001$.

6–reactive LNs of *Prf1*-deficient mice that had received a first transfer of N4-, Q4-, or T4-pulsed DCs and a subsequent transfer of either unpulsed DCs or equally pulsed DCs 60 h after T cell transfer. N4-primed OT-I T cells responded to secondary pMHC-driven DC encounters with increased cell size (assessed by forward scatter [FSC]) and CD25 expression (Fig. 5, A–C), hallmarks of ongoing proliferation. The percentage and total number of N4-primed OT-I T cells among total CD8$^+$ T cells was almost doubled by successive encounters with N4-pulsed DCs transferred at later time points (Fig. 5, D and E). We also observed a nonsignificant trend of additional Q4- or T4-primed OT-I T cell percentages after successive priming with pulsed DCs, suggesting that a few low affinity–primed T cells retained signal integration capacity (Fig. 5 D). However, this did not result in significantly increased OT-I T cell populations on day 6 (Fig. 5 E), as the vast majority of the low-affinity progeny had acquired effector functions and egressed from lymphoid tissue at this time point.

CXCR3 expression is required for redistribution to IFRs and integration of successive DC signals

IFRs serve as migratory corridors for DCs arriving from the periphery (Schumann et al., 2010; Ulvmar et al., 2014). To examine the relevance of CXCR3 expression for OT-I T cell redistribution to IFRs, we used SPIM to localize GFP$^+$ CXCR3$^{-/-}$ OT-I T cells in day 3–reactive LNs after N4-induced expansion. Lack of CXCR3 did not significantly alter early OT-I T cell activation as measured by CD25 expression (not depicted) or the medullary–cortical distribution as compared with CXCR3$^{+/+}$ OT-I T cells (Fig. 6, A and B). However, 3D reconstructions of entire LNs and analysis of centroid positions showed that CXCR3$^{-/-}$ OT-I T cells were impaired in their ability to redistribute to IFRs (Fig. 6, A and C; and Video 12).

Next, we investigated the relevance of CXCR3 expression for signal integration from sustained DC encounters. 60 h after T cell transfer, we transferred a second wave of N4-pulsed

Published October 31, 2016

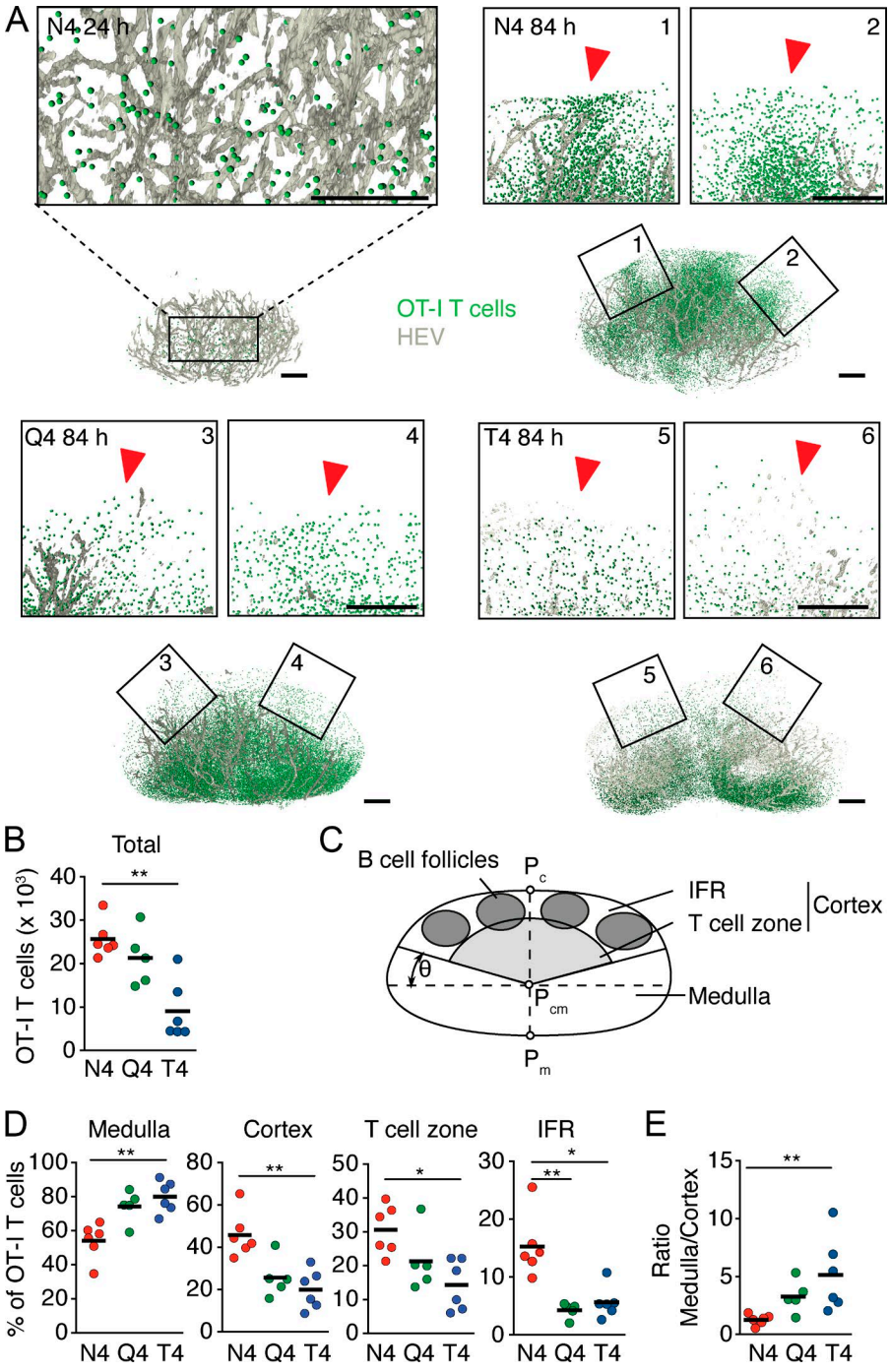

Figure 4. **TCR affinity governs OT-I T cell localization during expansion.** (A–E) LNs were isolated 24 or 84 h after transfer of 10^4 GFP$^+$ OT-I T cells into *Prf1*-deficient mice containing N4-, Q4-, or T4-pulsed DCs and analyzed by SPIM. (A) 3D volume rendering of the HEV network (gray) and GFP$^+$ OT-I T cells (green) at 24 h (only for N4) and 84 h in LNs containing N4-, Q4-, or T4-pulsed DCs. Higher magnification images show OT-I T cell localization in the T cell zone (24-h LNs) or IFRs (84-h LNs; red arrowheads). Bars, 300 µm. Data are representative of three independent experiments with four mice at 84 h and one experiment at 24 h after T cell transfer. (B) Total OT-I T cell numbers per LN 84 h after T cell transfer. (C) 3D quantification scheme of SPIM-generated datasets. Cortical position (P_c), medullary position (P_m), and cortical-medullary position (P_{cm}), together with the polar angle θ fixed at 20°, were used to subdivide 3D LN renderings into microenvironments as described in Fig. S1. (D) The percentage of total OT-I T cells that was detected within medulla, cortex, T cell zone, and IFRs. (E) Medulla/cortex ratio of OT-I T cells. (B–E) Data are pooled from three independent experiments with total of five to six LNs isolated from total of four mice per condition. (B, D, and E) Each dot represents one LN. Statistical significance was analyzed by Kruskal-Wallis tests with Dunn's posttest. *, $P < 0.05$; **, $P < 0.01$.

or unpulsed control DCs into *Prf1*-deficient mice that contained N4-primed CXCR3$^{+/+}$ or CXCR3$^{-/-}$ OT-I T cells and analyzed OT-I T cell expansion on day 6. Late-arriving N4-pulsed DCs resulted in lower rise in the frequency of FSC^{high} and CD25-expressing CXCR3$^{-/-}$ OT-I as compared with CXCR3$^{+/+}$ OT-I T cells (Fig. 6, D and E), with a non-significant trend for lower CD25 MFI (Fig. 6 F). As a result, the percentage of CXCR3$^{-/-}$ OT-I T cells recovered on day 6 from reactive LNs was significantly decreased as compared with CXCR3$^{+/+}$ OT-I T cells (Fig. 6 G). In sum, CXCR3 expression on activated CD8$^+$ T cells is required for efficient signal integration during late encounters with pMHC-presenting DCs, correlating with their translocation to IFRs of reactive LNs.

Low affinity–primed CD8$^+$ T cells efficiently eliminate target cells outside reactive LNs at early time points

We investigated whether low affinity–primed CD8$^+$ T cells rapidly eliminate target cells outside their lymphoid priming

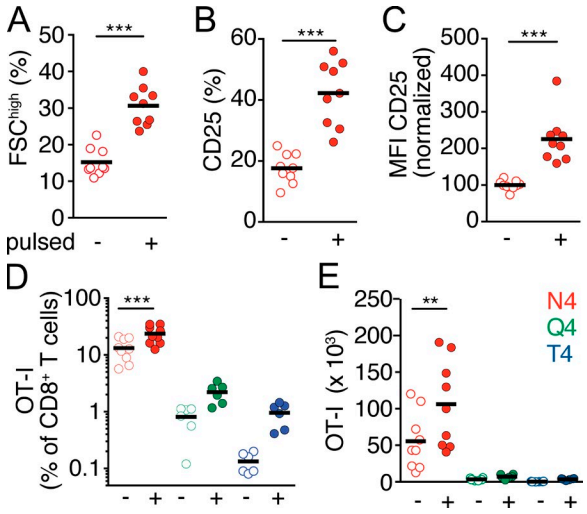

Figure 5. **Successive DC encounters lead to enhanced expansion in a TCR affinity–dependent manner.** (A–E) *Prf1*-deficient mice received s.c. injections of N4-, Q4-, and T4-pulsed DCs, followed by transfer of 10^4 GFP$^+$ OT-I T cells 1 d later. After 60 h, mice received a second wave of unpulsed or N4-, Q4-, or T4-pulsed DCs. Flow cytometry was performed on day 6. (A) Percentage of FSC^{high} cells on day 6 after transfer. (B and C) Percentage of CD25$^+$ OT-I T cells (B) and CD25 MFI levels (normalized to unpulsed DC-exposed OT-I T cell values; C). (A–C) Data are pooled from three independent experiments with total of nine mice per condition. (D and E) Percentage (D) and total cell numbers (E) of OT-I T cells on day 6 after a second transfer of unpulsed or peptide-pulsed DCs 60 h after T cell transfer. Data are pooled from two independent experiments with total of six mice per condition. Bars show the mean. Statistical significance was analyzed by Mann-Whitney (A–C) or Kruskal-Wallis tests with Sidak's posttest (D and E). **, $P < 0.01$; ***, $P < 0.001$.

tissue because of their earlier release into the circulation and acquisition of effector function (Zehn et al., 2009). We s.c. injected unpulsed DCs together with N4-, Q4-, or T4-pulsed DCs into previously immunized mice at sites that drained into reactive popliteal or nonreactive brachial LNs and quantified DC recovery from both types of LNs (Fig. 7 A). We failed to detect killing of pulsed DC in nonreactive LNs 84 h after T cell transfer, whereas Q4- and in particular T4-primed OT-I effector T cells were efficiently eliminating pulsed DCs on a per-cell basis in reactive LNs (Fig. 7, B–D), as in Fig. 2. At 108 h after primary activation, we observed a skewed unpulsed to pulsed DC ratio in nonreactive LNs, indicative of antigen-dependent DC elimination (Fig. 7 D). Similar to reactive LNs, Q4- and T4-primed OT-I T cells showed superior per-cell killing efficacy in nonreactive LNs 108 h after primary activation as compared with N4-primed OT-I T cells (Fig. 7 E). Furthermore, the ratio of low to high affinity–primed OT-I T cells was relatively increased in brachial versus popliteal LNs, suggesting earlier egress of low-affinity T cells (not depicted). These findings support the hypothesis that, at early time points, the progeny of low affinity–primed CD8$^+$ T cells egress reactive LNs earlier and possess higher per-cell cytotoxic function than high affinity–primed T cell progeny. APL-primed OT-I T cells also efficiently eliminated N4-pulsed DCs injected into the front footpad, ruling out an influence of Q4 or T4 pulsing on effector OT-I cytotoxic activity (not depicted).

Low affinity–primed CD8$^+$ T cells provide early protection during local viral infection

We examined whether key aspects of our DC immunization data were recapitulated during a microbial challenge. We infected C57BL/6 hosts that had received cotransferred OT-I and OT-3 T cells with an attenuated OVA-expressing lymphocytic choriomeningitis virus (LCMV-OVA; Fig. 8 A). On day 2 p.i., OT-3 T cells displayed a lower percentage of CD69$^+$ and CXCR3$^+$ cells and decreased normalized MFI compared with OT-I T cells (Fig. 8, B and C). Although virtually all OT-I and OT-3 T cells expressed GzmB, presumably owing to the strong proinflammatory environment caused by viral danger signals, normalized *GzmB* mRNA levels were significantly higher on OT-3 as compared with OT-I T cells at this early time point (Fig. 8 D). On day 7 p.i., this difference in *GzmB* mRNA levels disappeared, consistent with the full differentiation of high affinity–primed effector cells (not depicted). These results are consistent with controlled DC immunization schemes and support the spatiotemporal model of T cell affinity maturation on a population level (Fig. S2).

Finally, we explored whether early effector function acquisition of low-affinity T cells contributes to microbial containment in a local infection model. We transferred OT-I and OT-3 T cells separately into *Prf1*-deficient recipients and infected their skin with a tdTomato- and OVA-expressing HSV, $HSV_{TOM\text{-}OVA}$ (Fig. 8 E). In this model, viral titers peaked between days 2 and 3 p.i. in WT mice (Ariotti et al., 2015). On day 2.5 p.i., we isolated infected skin and determined viral titers. As predicted, $HSV_{TOM\text{-}OVA}$ titers escalated in *Prf1*-deficient mice that had received no CD8$^+$ T cells (Fig. 8 F). When we transferred 5×10^4 OT-I T cells, no significant early protection against HSV-1 was detected at 60 h after transfer (Fig. 8 F). Because recent improvements in measuring antigen-specific T cell frequencies have uncovered previously unnoticed low-affinity CD8 T cell precursors that outnumber high-affinity precursors by a factor of ≥10 (Huang et al., 2016), we compared the HSV-1 titers after transfer of 5×10^5 OT-3 T cells and the same number of OT-I T cells. At the early time point measured, OT-3 T cells showed a significantly improved viral containment as compared with 5×10^4 and to a lesser extent with 5×10^5 OT-I T cells (Fig. 8 F). This finding suggests that low-affinity T cells contribute to an unexpectedly rapid and effective early antimicrobial response in a local infection model.

DISCUSSION

During the expansion phase of adaptive immune responses, clonal proliferation and effector differentiation result in an early release of effector T cells with broad TCR affinities, followed by preferential expansion of high-affinity T cells (Zehn

Published October 31, 2016

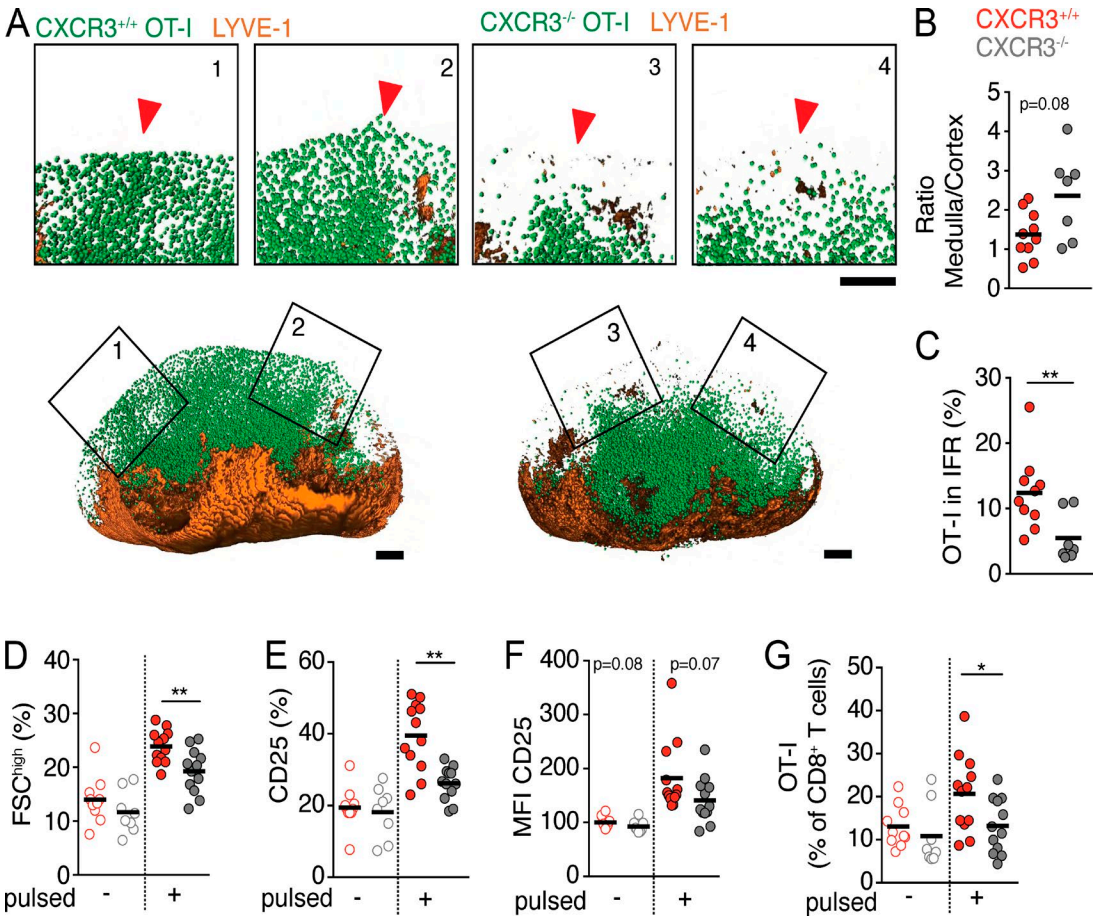

Figure 6. **CXCR63 is required for efficient signal integration from successive DC encounters.** (A–C) GFP$^+$ CXCR3$^{+/+}$ or CXCR3$^{-/-}$ OT-I T cells (10^4/mouse) were transferred into *Prf1*-deficient mice that contained N4-pulsed DCs. At 84 h after T cell transfer, LNs were isolated and analyzed by SPIM. (A) 3D volume rendering of LYVE-1$^+$ lymphatic vessel network (red) and GFP$^+$ CXCR3$^{+/+}$ or CXCR3$^{-/-}$ OT-I T cells (green). Higher magnification images show the indicated IFRs (red arrowheads). Bars, 300 µm. Data are representative of two independent experiments with two mice. (B and C) Medulla/cortex ratio (B) and percentage of CXCR3$^{+/+}$ and CXCR3$^{-/-}$ OT-I T cells in IFRs over total cell number (C). Data are pooled from at least two independent experiments with total of 7–10 LNs isolated from four to six mice per condition. CXCR3$^{+/+}$ OT-I data are taken from Fig. 4 (D and E). (D) Percentage of FSC^{high} cells on day 6 after transfer. (E and F) Percentage of CD25$^+$ OT-I T cells (E) and CD25 MFI levels (normalized to unpulsed DC-primed CXCR3$^{+/+}$ OT-I T cell values; F). (G) Percentage of OT-I T cells on day 6 after a second transfer of unpulsed or N4-pulsed DCs 60 h after T cell transfer as in Fig. 5. (D–G) Data are pooled from three independent experiments with total of 8–12 LNs isolated from four to six mice per condition. (B–G) Bars show the mean, and dots represent data from individual LNs. Statistical significance was analyzed by Student's *t* tests. *, $P < 0.05$; **, $P < 0.01$.

et al., 2009). Here, we used a reductionist DC immunization approach to examine how TCR–pMHC affinity regulates initial CD8$^+$ T cell–DC interactions, intranodal localization of expanding daughter cells, and the timing of effector differentiation. We show that during the priming phase, CD8$^+$ T cells rapidly formed stable contacts with low-affinity pMHC-presenting DCs (phase 1 to 2 transition) but of shorter duration (phase 2 to 3 transition). Curtailed phase 2–type contacts with DCs correlated with decreased induction of BATF and IRF4, which control effector function acquisition and proliferation-related genes. Low-affinity peptide-primed OT-I T cells moved to medullary regions of reactive LNs and failed to redistribute to IFRs. In contrast, OT-I T cells primed with high-affinity N4 peptide efficiently relocalized to IFRs in a CXCR3-dependent manner, which in combination with delayed acquisition of effector functions allowed signal integration from newly incoming DCs and prolonged proliferation. In turn, the early release of low-affinity effectors contributed to containment of spreading viral infections.

Levels of pMHC determine the dynamic interaction patterns of cognate T cells and DCs, with low abundance leading to prolonged T cell scanning and signal integration before stable engagement (Henrickson et al., 2008). Similarly, we anticipated that low pMHC affinity would mostly affect prolonged phase 1–like T cell scanning, as observed by the impaired deceleration of CD8$^+$ T cells in the presence of APL-loaded DCs (Moreau et al., 2012; Pace et al., 2012). Although we confirmed a mild effect of low-affinity pMHC

Published October 31, 2016

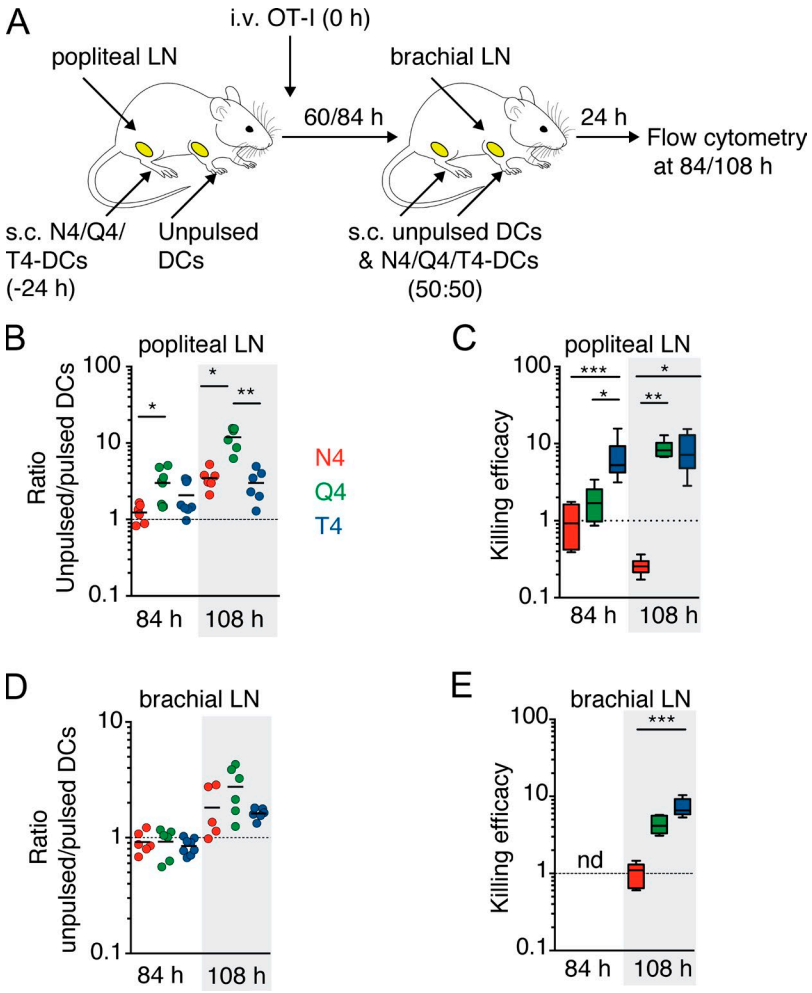

Figure 7. **Low affinity–primed T cells contribute to early elimination of target cells outside lymphoid priming tissue.** (A) *Prf1*-deficient mice received s.c. injections of N4-, Q4-, and T4-pulsed DCs into hind and unpulsed DCs into front footpads, followed by i.v. transfer of 10^4 GFP$^+$ OT-I T cells 24 h later. At 60 or 84 h after T cell transfer, mice received a second injection of mixed fluorescently labeled unpulsed and N4-, Q4-, or T4-pulsed DCs into hind and front footpads. Draining reactive popliteal and nonreactive brachial LNs were isolated 24 h later to determine DC elimination as in Fig. 2. (B and C) Ratio of unpulsed and pulsed DCs (B) and per-cell killing efficacy (C) in popliteal LNs at 84 and 108 h after T cell transfer. (D and E) Ratio of unpulsed and pulsed DCs at 84 and 108 h (D) and per-cell killing efficacy (E) in brachial LNs at 84 h after T cell transfer. (B–E) Data are pooled from two independent experiments with total of five to eight LNs isolated from three to four mice per condition. Statistical significance was analyzed by Kruskal-Wallis tests with Dunn's posttest. *, $P < 0.05$; **, $P < 0.01$; ***, $P < 0.001$.

on T cell deceleration, most parameters of early T cell–DC interactions remained remarkably similar irrespective of TCR–pMHC affinity. We observed comparable pMHC affinity–dependent CXCR3, CD69, and GzmB regulation on transferred OT-I T cells when we injected DCs pulsed with 10 nM peptide; however, recovery of APL-pulsed T cells was not consistently high enough for quantitative analysis (unpublished data). In our experimental system, all early T cell–DC interactions were predominantly long term, which enabled us to examine the correlation between TCR affinity and overall duration of stable T cell–DC interactions. Whereas previous intravital imaging studies have focused on whether stable interactions (phase 1 to 2 transition) occur between T cells and DCs in the first place, the actual duration of stable interactions between T cells and DCs (length of phase 2) has so far not been comprehensively assessed to our knowledge. Our data show that TCR–pMHC affinity directly regulates the duration of continuous T cell–DC interactions that precede T cell detachment and proliferation. It remains unclear how affinity regulates prolonged interactions. Stronger TCR binding to high-affinity pMHC may translate into delayed detachment (Gronski et al., 2004). Alternatively, TCR affinity may have impact on the stability of the immunological synapse (Grakoui et al., 1999), e.g., by regulation of LFA-1 activity (Davis, 2009). In any event, the initial duration of T cell–DC contacts is likely to permit the continuous transcription of activation-induced gene products in T cells, and this early gene transcription activity is likely cut short after T cell release from DCs. Thus, IRF4 expression is quickly turned off when TCR signaling ceases (Man et al., 2013). BATF and IRF4 are pioneer transcription factors with both activating and inhibitory functions, which control expression of genes including *GzmB* and *CXCR3* and act within the first 24–72 h of initial TCR activation to balance proliferation and effector cell differentiation (Murphy et al., 2013; Godec et al., 2015). We found that prolonged T cell–DC interactions correlated with increased *Batf* and in particular *Irf4* mRNA levels. After detaching from DCs, when activated CD8$^+$ T cells begin dividing, the level of mRNA or protein accumulated during the DC contact–triggered transcriptional activity becomes diluted with each cell division until it falls below a threshold that switches on an effector differentiation program. In this simplistic scenario, low BATF and IRF4 expression in daughter cells of low- and medium-affinity pMHC-primed

Published October 31, 2016

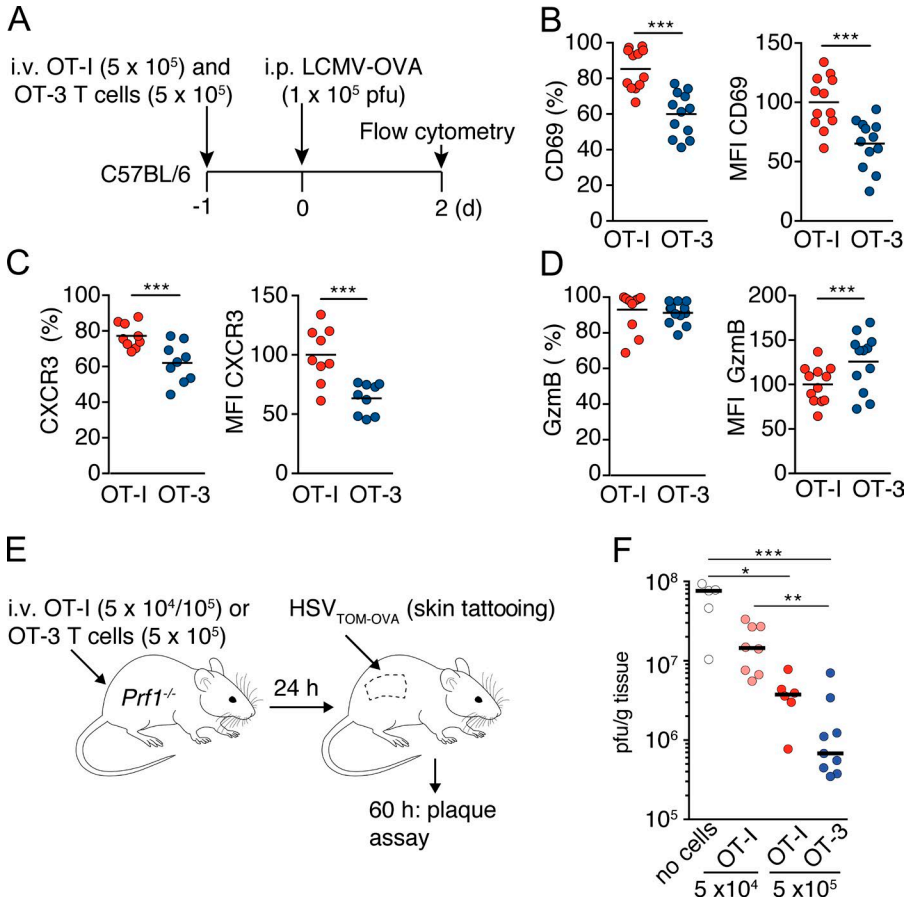

Figure 8. **Low-affinity T cells show reduced expression of CXCR3 and CD69 but increased gzmB at viral infection onset and contribute to early host protection.** (A) Experimental layout of systemic LCMV-OVA infection. (B–D) Percent positive and normalized MFI of CD69 (B), CXCR3 (C), and GzmB (D) expression of OT-I and OT-3 T cells at 48 h p.i. Data are pooled from three to four independent experiments with a total of 9–12 mice per condition. Statistical significance was analyzed by paired Student's *t* tests. (E) Experimental layout of local $HSV_{TOM-OVA}$ skin infection. (F) Viral titers (as determined by PFU/gram of tissue) in skin tissue of *Prf1*-deficient mice that had not received T cells versus recipients of 5×10^4 or 5×10^5 OT-I and OT-3 T cells. Data are pooled from three independent experiments with five to nine mice total (for no cells and 5×10^5 T cell recipients) and one experiment (5×10^4 T cell recipients) with four mice. Each point represents one skin biopsy. Bars indicate the median. Statistical significance was analyzed using a Kruskal-Wallis test against no cells with Dunn's posttest. *, $P < 0.05$; **, $P < 0.01$; ***, $P < 0.001$.

$CD8^+$ T cells causes their early acquisition of effector gene expression and cytotoxic function (Fig. S2). Our data support a model in which TCR signaling promotes an early digital response, i.e., arrest versus continuous scanning, which is subsequently scaled in an analogue manner to affinity-dependent signal strength by controlling TCR signal duration (Tkach and Altan-Bonnet, 2013). Digital all-or-none behavior fits well with early signaling properties of the TCR (Altan-Bonnet and Germain, 2005), whereas our data show the importance of sustained TCR signaling during the earliest priming phase as an analogue rheostat for appropriate expansion (van Heijst et al., 2009; Tkach and Altan-Bonnet, 2013).

Recent elegant experiments have shown that single CD8 T cells display a high heterogeneity in their response patterns during a microbial infection, with some cells undergoing massive expansion and others with very limited proliferative responses (Buchholz et al., 2013; Gerlach et al., 2013; Plumlee et al., 2013). Only when averaging dozens of single-cell fates does a consistent pattern of OT-I expansion and differentiation emerge. We hypothesize that TCR affinity for pMHC shifts these individual fates toward cells with massive (N4) or limited (Q4 and T4) expansion, yet with considerable overlap. At later stages in reactive LNs, the few Q4- and T4-stimulated OT-I T cells, which have had the most proliferative response (and therefore least cytotoxic T cell differentiation), will become enriched. In agreement with this, we observed in our 2PM studies a minor fraction of OT-I T cells still engaged in prolonged interactions with T4-pulsed DCs in the 24–32-h time window after T cell transfer. It is likely that some of these late interactors remain longer in LNs and are able to integrate additional signals by newly incoming DCs. Yet, the effect of late encounters with antigen-presenting cells appears far less important for low affinity–primed effector T cells on a population level because most have acquired cytotoxic activity coinciding with their earlier egress from LNs as first wave effectors, leaving behind only very few responding cells. In contrast, signal-integrating high-affinity T cell clone populations continuously expand and dominate immune responses >1 wk after infection. An interesting field for future analysis is whether mechanisms controlling T cell heterogeneity during activation with a single peptide follow comparable patterns as the pMHC-affinity variability measured here, i.e., by differences in integrating DC interaction times.

Low-affinity T cell–DC interactions led to a daughter T cell localization pattern that favors egress. Using SPIM-based 3D reconstructions and novel image analysis tools to avoid limitations inherent to 2D tissue sections (Ludewig et al., 2012), we observed a striking accumulation of T4-primed OT-I T cell progeny in LN medulla, whereas N4-primed OT-I T cells were primarily in the cortical and peripheral

regions 3–4 d after expansion. Q4-primed OT-I T cells showed an intermediate phenotype but were mostly found in the medulla. This pattern of localization correlated well with decreased CD69 and increased S1P1 expression patterns in Q4- and T4-primed cells as compared with N4-primed cells. Recent in vitro studies have shown that CXCR3 expression is rapidly induced on $CD8^+$ T cells during primary stimulation in a pMHC affinity–dependent manner (Preston et al., 2013). We show that, also in vivo, N4-primed OT-I T cells showed the highest CXCR3 expression and moved to the outer cortical regions of LNs in a CXCR3-dependent manner, although in our hands, we were unable to detect CXCL9 or CXCL10 in LN sections (unpublished data). In combination with low T cell migration to CXCL10, CXCL9 expressed in IFRs appears to play a dominant role in creating intranodal CXCR3 ligand gradients in our DC immunization model (Groom et al., 2012).

After clearance of an infection, central memory $CD8^+$ T cells remain in SLOs and use CXCR3 to localize or accumulate in IFRs, which during immune responses express the CXCR3 ligands CXCL9 and CXCL10 (Groom et al., 2012; Sung et al., 2012; Kastenmüller et al., 2013). IFRs constitute a specialized microenvironment in LNs containing innate immune cells, also serving as a migratory corridor for activated DCs arriving via afferent lymphatic vessels (Schumann et al., 2010; Ulvmar et al., 2014). CXCR3-dependent localization allows central memory $CD8^+$ T cells to quickly intercept incoming DCs, leading to more efficient recall responses. Our data show that this is not a unique feature of central memory $CD8^+$ T cells but already occurs during the primary DC-induced expansion of $CD8^+$ T cells and contributes to signal integration and expansion (Marchingo et al., 2014), similar to virus-triggered recruitment of naive T cells to subcapsular regions (Hickman et al., 2008). Peripheral accumulation of high affinity–primed T cells in IFRs may permit them to intercept newly arriving DCs for signal integration before they become targets of low affinity–primed effector T cells of the T cell zone and medulla. Although we have used here an artificial second transfer of pulsed DCs to simultaneously assess signal integration and cytotoxic activity in a controlled manner, recent studies support prolonged DC accumulation in draining LNs during an insult (Bedoui et al., 2009; Tomura et al., 2014; Kitano et al., 2016). In 2PM experiments, we noticed that expanded OT-I effector T cells were able to move between the T cell zone and IFRs, suggesting that there is constant treadmilling and exposure to microenvironmental factors. This may also explain why CXCR3-deficient OT-I T cells show reduced expansion during sustained DC stimulation, although only 15% of control OT-1 T cells located to IFRs at a given moment during expansion. IFRs contain abundant proinflammatory cytokines (Kastenmüller et al., 2012), which may favor prolonged high-affinity T cell expansion. Additionally, CXCR3 ligands may act as co-stimulatory factors within or outside IFRs (Dar and Knechtle, 2007; Newton et al., 2009) or favor interactions with CXCL9-producing DCs (Friedman et al., 2006). Successive encounters with DCs contribute to high affinity–primed T cell expansion and correlate with increased CD25 expression. CD25 signaling most likely contributes to the boost of OT-I T cell accumulation through sustained expression of cell cycle genes and proteins (Starbeck-Miller et al., 2014).

During viral infections, CXCR3 favors the differentiation of short-lived effector cells (Hu et al., 2011; Kohlmeier et al., 2011; Kurachi et al., 2011). In the DC immunization protocol used here, we did not observe short-lived effector cell formation in reactive LNs, presumably owing to lack of a highly proinflammatory cytokine environment, although we observed decreased CD127 expression after secondary stimulation (unpublished data). Furthermore, although a short DC stimulation suffices for effector cell differentiation, we have not explored how continuous DC signaling affects memory T cell formation. In any event, our early time point analysis of expanded OT-3 T cells during a viral infection, in combination with intravital imaging data, supports the basic concept of early egress and faster acquisition of cytotoxic activity as an inverse function of affinity. This was accompanied by effective early elimination of HSV-infected skin cells, which was already manifest within <3 d p.i. in the spatially constrained infection model used here. This unexpected fast kinetics may be caused by the supraphysiological numbers of T cells transferred in this infection model and the strong inflammatory response of infected skin, presumably leading to efficient recruitment of effector T cells. Furthermore, activated $CD8^+$ T cells continue to divide at effector sites (Kang et al., 2011), which may also occur in our model after a first priming in draining LNs. Although at 60 h p.i. the highly inflamed skin precluded a microscopic or flow cytometry analysis of infiltrating T cells, our observation that viral titers were significantly higher in mice that had not received antigen-specific T cells strongly suggests that adoptively transferred low-affinity T cells had already started to accumulate in the skin at this time point and challenges the view that T cell responses require 5–7 d to become apparent. In agreement with our HSV-1 model, a reassessment of our previous data using *Listeria monocytogenes* confirmed a higher early per-cell killing activity of early egressing low-affinity V4 peptide–primed as compared with N4-primed OT-I T cells (Zehn et al., 2009). Our data suggest that this is a transient, early effect, as at later time points, the progeny of high affinity–primed T cells exhibit comparable GzmB levels as low affinity–primed T cells. These data imply that low affinity–primed T cells serve as a first line of defense to contain the spread of fast-replicating microbes before large numbers of high-affinity T cell clones eliminate the remaining viral reservoirs.

In summary, we provide a model underlying functional avidity maturation of T cell responses during the course of an immune response. At the peak of effector responses, often measured after ≥1 wk of initiation of immune responses, a limited number of high-affinity clones dominates the adaptive immune response and has therefore been most extensively

Published October 31, 2016

studied. However, recent studies showed that numerous low TCR affinity–bearing T cells are found at sites of inflammation (Sabatino et al., 2011). Furthermore, a broad TCR repertoire encompassing varying TCR affinities helps to constrain viral escape mutants, contributes to the effector/memory T cell pool, and is beneficial in antitumor activity (Zehn et al., 2009; van Gisbergen et al., 2011; Blanchfield et al., 2013). Our studies add a further aspect to this notion by showing the accelerated acquisition of cytotoxicity by low-affinity T cells. Because low-affinity T cell clones initially outnumber high-affinity ones during priming, their combined populations of early released efficient killers are likely to contribute to host protection before high-affinity clones become dominant. This suggests that the adaptive immune system has evolved to rapidly produce early cytotoxic effector cells at the expense of extensive cell division. This dichotomy of either a strong proliferative response versus effector cell differentiation is reminiscent of developmental processes in other biological systems where proliferation and differentiation need to be carefully balanced (Hardwick and Philpott, 2014).

MATERIALS AND METHODS

Mice

C57BL/6 mice were purchased from Janvier (AD Horst). *Prf1*-deficient and CD45.1 mice were provided by the Institut für Labortierkunde, University of Zürich, Switzerland. GFP^+ OT-I mice were generated by crossing C57BL/6-Tg(-CAG-EGFP)131Osb/LeySopJ with $Rag2^{-/-}$ OT-I transgenic mice (provided by F. Ronchi, Institute for Research in Biomedicine, Bellinzona, Switzerland). GFP^+ $CXCR3^{-/-}$ OT-I transgenic mice were generated by crossing GFP^+ OT-I transgenic mice with $CXCR3^{-/-}$ mice (Hancock et al., 2000). OT-3 mice were described previously (Enouz et al., 2012). All mice were maintained in specific pathogen–free conditions at the Department of Clinical Research animal facility of the University of Bern. All animal work has been approved by the Cantonal Committee for Animal Experimentation and conducted according to federal guidelines.

T cell purification

Peripheral LNs and spleens from GFP^+ WT ($CXCR3^{+/+}$) and $CXCR3^{-/-}$ OT-I or OT-3 mice were harvested and homogenized using a 70-µm cell strainer. Untouched $CD8^+$ T cells were isolated with an EasySep Mouse $CD8^+$ T cell negative selection kit according to the manufacturer's protocol (STEMCELL Technologies). $CD8^+$ T cell purity was typically >95%.

DC culture and peptide pulsing

DCs were in vitro differentiated from BM of C57BL/6 or CD45.1 mice as described previously (Moalli et al., 2014). During the final 24 h of culture, cells were stimulated with 1 µg/ml LPS (Sigma-Aldrich) and pulsed with 100 nM N4 (SIINFEKL), Q4 (SIIQFEKL), or T4 (SIITFEKL; ECM Microtechnologies) peptides for 45 min at 37°C. In some experiments, DCs were pulsed with 1 and 10 nM peptides.

2PM of popliteal LN

To study primary T cell–DC interactions, CMTMR- or CMAC-labeled peptide-pulsed DCs (10^6/mouse) were s.c. injected into the hind footpad of sex-matched C57BL/6 mice 24 h before i.v. adoptive transfer of 3×10^6 GFP-expressing OT-I T cells. In some experiments, CMAC- or CMTMR-labeled OT-3 T cells (3×10^6/mouse and 0.5×10^6 for low–precursor frequency experiments) were i.v. cotransferred. After 3 h, further homing of cells was blocked by i.p. injection of anti-CD62L mAb (100 µg/mouse Mel-14; Nanotools). At 2–10 h or 24–32 h after T cell transfer, the right popliteal LN of recipient mice was surgically prepared as previously described (Moalli et al., 2014).

To study secondary T cell encounters with DCs, 10^6 unlabeled peptide-pulsed DCs were s.c. injected into hind footpads of sex-matched *Prf1*-deficient mice 24 h before adoptive transfer of 10^4 GFP^+ OT-I T cells. After 24 h, further homing of cells was blocked by i.p. injection of anti-CD62L mAb. Recipient mice received an i.p. injection of 1 mg/kg FTY720 48 h after T cell transfer to counteract Mel-14–induced deflation of lymphoid tissue. We s.c. transferred a second wave of CMTMR-labeled peptide-pulsed DCs into recipient mice 84 and 108 h after T cell transfer. 1 d later, recipient mice were surgically prepared to expose the right popliteal LN as described in the beginning of this section.

2PM imaging was performed using a TrimScope 2PM system equipped with a fluorescence microscope (BX50WI; LaVision Biotec; Olympus) equipped with a 20× objective (NA 0.95; Olympus). 16-slice z stacks with 4-µm spacing of 250 × 250–µm field of views (FOVs) were acquired every 20 s for 30 min. Imaging was performed in the T cell zone as identified by the presence high endothelial venules (HEVs; labeled with Alexa Fluor 633–coupled MECA-79; 10 µg/mouse). Volocity software (PerkinElmer) was used to generate volume-rendered 4D movies and for semiautomated tracking of cell motility. Mean single-cell track speeds were calculated from the x,y,z coordinates of cell centroids using Matlab (The MathWorks; Mempel et al., 2004). Only T cell–DC interactions for which initiation and termination was observed during an image sequence or that lasted throughout the entire 30-min observation period were included in the analysis.

Flow cytometry

10^6 peptide-pulsed DCs were s.c. injected into hind footpads of sex-matched C57BL/6 mice 24 h before adoptive transfer of 2×10^4 GFP-expressing $CXCR3^{+/+}$ or $CXCR3^{-/-}$ OT-I T cells. On day 3 or 4 after T cell transfer, draining LNs were harvested and homogenized using 70-µm cell strainers. Fc receptors were blocked with purified anti-CD16/CD32 mAb (2.4G2) in FACS buffer (PBS with 1% FCS and 0.05% NaN_3) for 10 min. Cells were stained with fluorochrome-conjugated mAbs against CD8 (53-6.7), CXCR3 (CXCR3-173; RT for 30 min), CD62L (Mel-14; 4°C for 30 min), or CD25 (3C7; 4°C for 30 min) or with appropriate isotype controls. Alternatively, cells were stained with biotin-conjugated mAb

against CCR7 (4B12; 37°C for 30 min) followed by secondary staining with fluorochrome-conjugated streptavidin and mAb against CD8 (53-6.7; RT for 30 min). For counting of total cell numbers, Flow-Count fluorospheres were used according to the manufacturer's protocol (Beckman Coulter). For intracellular staining for GzmB, Fc receptors were blocked as described in the beginning of this section, and cells were stained with fluorochrome-conjugated mAbs against CD8 (53-6.7) and CD45.1 (A20), fixed with 4% paraformaldehyde (PFA) at 4°C for 20 min, permeabilized with Cytofix/CytoPerm (BD) for 20 min at 4°C, and incubated with fluorochrome-conjugated mAb against gzmB (GB11) or isotype control (MOPC-21). For CD69 expression analysis, 10^6 peptide-pulsed DCs were s.c. injected into hind footpads of sex-matched C57BL/6 mice 24 h before adoptive transfer of 10^6 e670-labeled GFP-expressing OT-I T cells. After 60 h, recipient mice were sacrificed, and draining LNs were harvested and homogenized using a 70-µm cell strainer. Fc receptors were blocked as described in the beginning of this section, and cells were stained with fluorochrome-conjugated mAbs against CD8 (53-6.7) and CD69 (H1.2F3) at 4°C for 30 min. For CXCR3, CD69, and GzmB analysis on OT-3 and OT-I T cells after DC immunization or LCMV-OVA infection, recipient mice were sacrificed and draining LNs or spleens were harvested and homogenized using 70-µm cell strainers. Fc receptors were blocked as described in the beginning of this section, and cells were stained with fluorochrome-conjugated mAbs against CD8 (53-6.7), CD45.1 (A20), CXCR3 (CXCR3-173), and CD69 (H1.2F3; RT for 30 min). Samples were fixed with 4% PFA at 4°C for 20 min. For intracellular staining for GzmB, Fc receptors were blocked as described in the beginning of this section, and cells were stained with fluorochrome-conjugated mAbs against CD8 (53-6.7) and CD45.1 (A20), fixed with 4% PFA at 4°C for 20 min, permeabilized with Cytofix/CytoPerm (BD) for 20 min at 4°C, and incubated with fluorochrome-conjugated mAb against GzmB (GB11) or isotype control (MOPC-21) for 30 min at 4°C. Samples were analyzed using a FACSCalibur flow cytometer (BD) and FlowJo software (Tree Star).

qPCR analysis

10^6 peptide-pulsed DCs were s.c. injected into hind footpads of sex-matched C57BL/6 mice 24 h before adoptive transfer of 10^5 e670-labeled GFP^+ OT-I T cells. After 60 h, draining LNs from two to three recipient mice per condition were pooled and homogenized. OT-I T cells that had undergone at least one cell division as assessed by e670 dilution were sorted on a FACSAria II flow cytometer (BD) and lysed in RNAbee reagent (Ambion). As controls, we isolated RNA from naive OT-I T cells. Total RNA was chloroform-extracted, precipitated with isopropanol in the presence of glycogen (Roche), washed with 75% ethanol, and dissolved in water. To remove endogenous DNA, samples were treated with rDNase I according to the manufacturer's protocol (DNA-free kit; Ambion). RNA was reverse transcribed using SuperScript III reverse transcriptase and random hexanucleotide primers following the manufacturer's instruction (Invitrogen). To control for nonspecific amplification of genomic DNA, no RT controls were included. Real-time RT-qPCR was performed using a ViiA 7 system and SYBR green PCR master mix (Eurogentec). Specific target sequences were amplified with the use of commercial RT2 qPCR primers for *Batf*, *Gzmb*, and *Prf1* (QIAGEN) or with self-designed primers for *Cxcr3* (forward, 5′-CCCAACCACAAGTGCCAAAG-3′; and reverse, 5′-TCACTAACCTCAAGGTACATGGC-3′), *Irf4* (forward, 5′-GCTCATCACAGCTCATGTGG-3′; and reverse, 5′-ACTCGTAGCCCCTCAGGAAA-3′), *S1pr1* (forward, 5′-CGTCTTGCAAAAGTGGTGCG-3′; and reverse, 5′-GAGAAACAGCAGCCTCGCTCA-3′), and ribosomal protein S16 (forward, 5′-GATATTCGGGTCCGTGTGA-3′; and reverse, 5′-TTGAGATGGACTGTCGGATG-3′; Eurogentec). S16 was used as a reference gene.

Chemotaxis assay

Mice were injected with 10^6/footpad DCs 24 h before adoptive transfer of 2×10^4 GFP^+ OT-I T cells. At 72 or 96 h (day 3 or 4) after T cell transfer, draining LNs were harvested and homogenized using a 70-µm cell strainer. 10^6/well of single-cell suspensions were added to 5-µm pore–size Transwell chambers (Costar) and allowed to migrate toward 20 nM CXCL9 or CXCL10 (PeproTech) for 2.5 h at 37°C. Input and migrated GFP^+ OT-I cells were enumerated by flow cytometry.

SPIM analysis

Preparation of LN samples. 10^6/footpad of N4-, Q4-, or T4-pulsed DCs were s.c. injected into hind footpads of sex-matched *Prf1*-deficient mice 24 h before adoptive transfer of 10^4 GFP^+ $CXCR3^{-/-}$ or $CXCR3^{+/+}$ OT-I T cells. 24 h later, further homing of cells was blocked by i.p. injection of 100 µg/mouse anti-CD62L mAb (Mel-14) to synchronize their dwelling time. After 48 h, recipient mice received i.p. injections of the functional S1P1 antagonist FTY720 (1 mg/kg) to counteract LN deflation caused by Mel-14 treatment while allowing S1P1-expressing cells to accumulate close to efferent lymphatics until this time point (Fig. 4). To mimic conditions used in 2PM experiments, we transferred CMTMR-labeled peptide-pulsed and e670-labeled unpulsed DCs at 60 h after OT-I T cell transfer. At the same time, lymphatic vessels and $CD35^+$ follicular dendritic cells (FDCs) were labeled by s.c. injection of Alexa Fluor 633–conjugated anti-CD35 mAb or Alexa Fluor 594–conjugated anti–LYVE-1–mAb (both at 5 µg/mouse) into hind footpads. In some cases, HEV networks were labeled by i.v. injection of Alexa Fluor 633–conjugated MECA79 mAb (Nanotools) 10 min before LN harvest. At 84 h after T cell transfer, reactive LNs were carefully excised and fixed in 4% PFA for 24 h before removing surrounding fat tissue under a stereomicroscope. Cleaned LNs were mounted in 2% ultrapure low-melting agarose and were optically cleared following the CUBIC (clear, unobstructed brain/body-imaging cocktails and computational analysis)

Published October 31, 2016

protocol, which preserves fluorescent protein function (Susaki et al., 2014).

LN scanning. CUBIC-2–immersed LNs were scanned using an in-house multispectral SPIM setup, with five laser lines for fluorescent excitation (405, 480, 561, 593.5, and 635 nm) and six detection filters (447/60, 490/40, 525/50, 593/46, 628/40, and 670/30). Customized software was developed for automated hardware control of multispectral image acquisition (4D-Nature). In some cases, samples were imaged in an alternate version of the in-house SPIM, with excitation lines at 405, 488, 543, 594, and 638 nm matched with 445/60, 525/50, 585/60, 624/40, and 700/75 detection filters. In both systems, excitation was through a 2.5×/0.07 N PLAN objective lens (Leica Biosystems), and the detection was via a 5×/0.12 N PLAN EPI lens (Leica Biosystems). The FOV was 1,321 × 1,734 µm (1,024 × 1,344 pixels), and the spacing between image planes was 5 or 10 µm. Typically, we recorded 200–400 image planes of adjacent FOVs of LNs, which were stitched to create a tiled scan using the ImageJ (National Institutes of Health) plugin 3D stitching with linear blending as the fusion method (Preibisch et al., 2009).

Quantification of 3D LN reconstructions. Reconstructed 3D datasets were analyzed using IMARIS software (Bitplane). DCs and GFP^+ OT-I T cells were identified using the IMARIS spot detection algorithm, providing x,y,z coordinates of transferred cells. In some cases, unpulsed DCs and HEV networks emitted in the same channel. To separate these signals, we segmented fluorescent structures using the IMARIS surface detection algorithm, which allowed us to distinguish HEVs from DCs based on area and volume of the identified surfaces. Filtered surfaces were subsequently used to create a masked channel that lacked HEV structures for the identification of unpulsed DCs using the IMARIS spot detection algorithm. LYVE-1^+ lymphatic vasculature, $CD35^+$ FDCs, and, in some cases, the HEV network were used to define cortical-medullary LN orientation. Based on careful visual inspection of 3D LN renderings, we placed a vertical axis (A_v) in the center of the LN with length L. We named the point of intersection of A_v with the cortical edge cortical position P_c, whereas medullary position (P_m) refers to the A_v intersection with the medullary edge. To distinguish medulla from cortex, we found the following protocol to best match LN 3D reconstructions. We assigned a cortical-medullary position (P_{cm}) as the position at 1/3 of A_v between P_m and P_c. Centroid positions of OT-I T cells were considered to be located in the LN medulla when they fell into the volume between P_m and P_{cm} that was defined by the polar angle θ fixed at 20° to a plane perpendicular to A_v at the P_{cm} intersection and covering the full 360 azimuthal angle. Centroid positions of OT-I T cells in the remaining volume were defined as located in the LN cortex. We subdivided the cortex into a P_{cm}-proximal T cell zone and distal IFR zone (because $CD8^+$ T cells do not enter B cell follicles before memory phase, we assumed that any cortical-distal cell is in IFRs). To generate a generally valid subdivision, we analyzed the median of the minimal distance between P_m and 8–12 clusters of $CD35^+$ FDCs/LN (as surrogates for B cell follicles) in four LNs. We then normalized this value to the corresponding distance between P_m and P_c to obtain the value of 0.6 ± 0.09 (mean ± SD), which was applied to all analyzed 3D LN reconstructions. Thus, 0.6L defines the maximal distance of cortical OT-I centroid positions from P_m that are classified as located in the T cell zone. Cortical OT-I T cell centroid positions outside the T cell zone were assigned to IFRs. Matlab scripts are available upon request.

Analysis of DC killing

$CD45.1^+$ DCs were labeled with 1.5 µM CFSE for 15 min at 37°C, followed by labeling with 0.5 µM e670 or 10 µM e670 for 20 min at 37°C. $e670^{hi}$ cells were left unpulsed, whereas $e670^{lo}$ cells were pulsed with 100 nM N4, Q4, or T4 peptide for 45 min at 37°C. After washing, a 50:50 mix of $e670^{hi}$ and $e670^{lo}$ DCs (10^6 total/footpad) were injected s.c. into hind and, where indicated, front footpads of sex-matched *Prf1*-deficient recipient mice that contained activated GFP^+ OT-I T cells. After 24 h, mice were sacrificed, and LNs were digested with collagenase/dispase/DNase I solution (Roche) in PBS for 30 min at 37°C. Collagenase activity was blocked by addition of 500 µl PBS containing 2 mM EDTA. Cell suspensions were passed through a 70-µm cell strainer, centrifuged, and stained with PE-conjugated anti-CD45.1 mAb (A20) for flow cytometry analysis.

Signal integration analysis by sustained DC encounters

10^6/footpad of peptide-pulsed DCs were s.c. injected into hind footpads of sex-matched *Prf1*-deficient mice 24 h before adoptive transfer of 10^4 GFP^+ $CXCR3^{+/+}$ or $CXCR3^{-/-}$ OT-I T cells. After 24 h, further homing of cells was blocked by injection of 200 µg/mouse Mel-14 mAb. At 60 h after T cell transfer, mice received a second transfer of 0.5 × 10^6/footpad of peptide-pulsed DCs. On day 6 after T cell transfer, recipient mice were sacrificed, and draining LNs were harvested and homogenized. Cell suspensions were labeled with anti-CD16/CD32 mAb in FACS buffer to block Fc receptors before staining with fluorescently labeled mAbs against CD8 (53-6.7), CD25 (3C7; 4°C for 30 min), or appropriate isotype controls. For counting of total cell numbers, Flow-Count fluorospheres were used according to the manufacturer's protocol (Beckman Coulter).

Viral infections

OVA-expressing recombinant LCMV-OVA was generated according to established procedures (Emonet et al., 2009; Flatz et al., 2010). C57BL/6 mice were adoptively transferred with GFP^+ OT-I T cells and $CD45.1^+$ OT-3 T cells (5 × 10^5 of each). 24 h later, mice were i.p. infected with 10^5 PFU LCMV-OVA. 2 or 7 d after infection, spleens were harvested, homogenized using 70-µm cell strainers to obtain single-cell

suspensions, stained, and analyzed using a FACSCalibur cell analyzer (BD) and FlowJo software (Tree Star). For HSV infections, OT-I or OT-3 T cells (5×10^4 or 5×10^5/mouse) were adoptively transferred into *Prf1*-deficient mice. 1 d later, intraepithelial infection was carried out on shaved flanks of anesthetized mice by tattooing a 10-µl droplet containing 5×10^5 PFU $HSV_{TOM\text{-}OVA}$ (provided by T.N. Schumacher, Netherlands Cancer Institute, Amsterdam, Netherlands) encoding tandem dimer tomato and OVA onto the skin using a sterile disposable nine-needle bar mounted on a rotary tattoo device as described previously (Ariotti et al., 2015). 60 h after infection, viral loads in infected skin were measured in 10-mm punch biopsies enclosing the entire infected area. Vero cells were seeded in six-well plates at a density of 4×10^5 cells per well such that monolayers were confluent the following day and infected with serial dilutions of homogenized skin (MagNA Lyser; Roche) for 45 min. After incubation in medium containing 0.5% methylcellulose for 72 h, plaques were identified by 0.1% crystal violet staining and counted.

Statistical analysis

Data were analyzed using Prism 6 (GraphPad Software) using unpaired or paired Student's *t* tests or Mann-Whitney or Kruskal-Wallis tests followed by Dunn's posttest. P-values <0.05 were considered significant.

Online supplemental material

Fig. S1 shows the quantification protocol developed for 3D SPIM reconstructions of entire LNs. Fig. S2 depicts a graphical summary of our findings. Videos 1–6 show OT-I T cell interactions with N4-, Q4-, or T4-pulsed DCs at early (2–10 h after T cell transfer) or late (24–32 h) time points. Videos 7 and 8 show OT-I and OT-3 T cell interactions with N4-pulsed DCs at early (2–10 h after T cell transfer) or late (24–32 h) time points, respectively. Videos 9–11 show 3D SPIM reconstructions of entire LNs containing N4-, Q4-, or T4-primed OT-I T cells at day 3 after T cell transfer. Video 12 shows a 3D SPIM reconstruction of entire LNs containing N4-primed $CXCR3^{-/-}$ OT-I T cells at day 3 after T cell transfer.

ACKNOWLEDGMENTS

We thank Feline Dijkgraaf, Silvia Ariotti, and Ton N. Schumacher for valuable advice and materials for HSV-1 infection. Microscopy was performed on equipment supported by the Microscopy Imaging Center, University of Bern, Switzerland. The SPIM setup was supported by the Pierre Mercier Foundation.

This work was supported by a Novartis Research grant (to A.J. Ozga) and Swiss National Science Foundation grants (31003A_135649 and CR23I3_156234 to J.V. Stein and CRSII3_141918 to J.V. Stein and J. Sharpe). J. Ripoll acknowledges support from European Commission FP7 Career Integration Grants (HIGH-THROUGHPUT TOMO), European Commission FP7 Marie Curie Actions (grant 2PM), and the Ministerio de Economía y Competitividad (grant FIS2013-41802-R). J. Sharpe acknowledges support from the Ministerio de Economía y Competitividad, Centro de Excelencia Severo Ochoa 2013–2017 (grant SEV-2012-0208).

The authors declare no competing financial interests.

Author contributions: A.J. Ozga, F. Moalli, J. Abe, and J. Swoger performed experiments. J. Sharpe, D. Zehn, M. Kreutzfeldt, D. Merkler, and J. Ripoll provided vital material and image acquisition hardware and software. J. Ripoll wrote scripts for SPIM-based analysis. A.J. Ozga and J.V. Stein wrote the manuscript with input from all coauthors.

Submitted: 10 February 2016
Revised: 1 July 2016
Accepted: 30 September 2016

REFERENCES

Abe, J., A.J. Ozga, J. Swoger, J. Sharpe, J. Ripoll, and J.V. Stein. 2016. Light sheet fluorescence microscopy for in situ cell interaction analysis in mouse lymph nodes. *J. Immunol. Methods.* 431:1–10. http://dx.doi.org/10.1016/j.jim.2016.01.015

Altan-Bonnet, G., and R.N. Germain. 2005. Modeling T cell antigen discrimination based on feedback control of digital ERK responses. *PLoS Biol.* 3:e356. http://dx.doi.org/10.1371/journal.pbio.0030356

Ariotti, S., J.B. Beltman, R. Borsje, M.E. Hoekstra, W.P. Halford, J.B.A.G. Haanen, R.J. de Boer, and T.N.M. Schumacher. 2015. Subtle CXCR3-dependent chemotaxis of CTLs within infected tissue allows efficient target localization. *J. Immunol.* 195:5285–5295. http://dx.doi.org/10.4049/jimmunol.1500853

Bedoui, S., P.G. Whitney, J. Waithman, L. Eidsmo, L. Wakim, I. Caminschi, R.S. Allan, M. Wojtasiak, K. Shortman, F.R. Carbone, et al. 2009. Cross-presentation of viral and self antigens by skin-derived $CD103^+$ dendritic cells. *Nat. Immunol.* 10:488–495. http://dx.doi.org/10.1038/ni.1724

Blanchfield, J.L., S.K. Shorter, and B.D. Evavold. 2013. Monitoring the dynamics of T cell clonal diversity using recombinant peptide:MHC technology. *Front. Immunol.* 4:170. http://dx.doi.org/10.3389/fimmu.2013.00170

Buchholz, V.R., M. Flossdorf, I. Hensel, L. Kretschmer, B. Weissbrich, P. Gräf, A. Verschoor, M. Schiemann, T. Höfer, and D.H. Busch. 2013. Disparate individual fates compose robust $CD8^+$ T cell immunity. *Science.* 340:630–635. http://dx.doi.org/10.1126/science.1235454

Busch, D.H., and E.G. Pamer. 1999. T cell affinity maturation by selective expansion during infection. *J. Exp. Med.* 189:701–710. http://dx.doi.org/10.1084/jem.189.4.701

Cullen, S.P., and S.J. Martin. 2008. Mechanisms of granule-dependent killing. *Cell Death Differ.* 15:251–262. http://dx.doi.org/10.1038/sj.cdd.4402244

Curtsinger, J.M., C.M. Johnson, and M.F. Mescher. 2003. CD8 T cell clonal expansion and development of effector function require prolonged exposure to antigen, costimulation, and signal 3 cytokine. *J. Immunol.* 171:5165–5171. http://dx.doi.org/10.4049/jimmunol.171.10.5165

Daniels, M.A., E. Teixeiro, J. Gill, B. Hausmann, D. Roubaty, K. Holmberg, G. Werlen, G.A. Holländer, N.R.J. Gascoigne, and E. Palmer. 2006. Thymic selection threshold defined by compartmentalization of Ras/MAPK signalling. *Nature.* 444:724–729. http://dx.doi.org/10.1038/nature05269

Dar, W.A., and S.J. Knechtle. 2007. CXCR3-mediated T-cell chemotaxis involves ZAP-70 and is regulated by signalling through the T-cell receptor. *Immunology.* 120:467–485. http://dx.doi.org/10.1111/j.1365-2567.2006.02534.x

Davis, D.M. 2009. Mechanisms and functions for the duration of intercellular contacts made by lymphocytes. *Nat. Rev. Immunol.* 9:543–555. http://dx.doi.org/10.1038/nri2602

Emonet, S.F., L. Garidou, D.B. McGavern, and J.C. de la Torre. 2009. Generation of recombinant lymphocytic choriomeningitis viruses with trisegmented genomes stably expressing two additional genes of interest. *Proc. Natl. Acad. Sci. USA.* 106:3473–3478. http://dx.doi.org/10.1073/pnas.0900088106

Enouz, S., L. Carrié, D. Merkler, M.J. Bevan, and D. Zehn. 2012. Autoreactive T cells bypass negative selection and respond to self-antigen stimulation during infection. *J. Exp. Med.* 209:1769–1779. http://dx.doi.org/10.1084/jem.20120905

Flatz, L., A.N. Hegazy, A. Bergthaler, A. Verschoor, C. Claus, M. Fernandez, L. Gattinoni, S. Johnson, F. Kreppel, S. Kochanek, et al. 2010. Development

of replication-defective lymphocytic choriomeningitis virus vectors for the induction of potent CD8+ T cell immunity. *Nat. Med.* 16:339–345. http://dx.doi.org/10.1038/nm.2104

Friedman, R.S., J. Jacobelli, and M.F. Krummel. 2006. Surface-bound chemokines capture and prime T cells for synapse formation. *Nat. Immunol.* 7:1101–1108. http://dx.doi.org/10.1038/ni1384

Gerlach, C., J.C. Rohr, L. Perié, N. van Rooij, J.W.J. van Heijst, A. Velds, J. Urbanus, S.H. Naik, H. Jacobs, J.B. Beltman, et al. 2013. Heterogeneous differentiation patterns of individual CD8+ T cells. *Science.* 340:635–639. http://dx.doi.org/10.1126/science.1235487

Germain, R.N., M.J. Miller, M.L. Dustin, and M.C. Nussenzweig. 2006. Dynamic imaging of the immune system: progress, pitfalls and promise. *Nat. Rev. Immunol.* 6:497–507. http://dx.doi.org/10.1038/nri1884

Godec, J., G.S. Cowley, R.A. Barnitz, O. Alkan, D.E. Root, A.H. Sharpe, and W.N. Haining. 2015. Inducible RNAi in vivo reveals that the transcription factor BATF is required to initiate but not maintain CD8+ T-cell effector differentiation. *Proc. Natl. Acad. Sci. USA.* 112:512–517. http://dx.doi.org/10.1073/pnas.1413291112

Grakoui, A., S.K. Bromley, C. Sumen, M.M. Davis, A.S. Shaw, P.M. Allen, and M.L. Dustin. 1999. The immunological synapse: a molecular machine controlling T cell activation. *Science.* 285:221–227. http://dx.doi.org/10.1126/science.285.5425.221

Gronski, M.A., J.M. Boulter, D. Moskophidis, L.T. Nguyen, K. Holmberg, A.R. Elford, E.K. Deenick, H.O. Kim, J.M. Penninger, B. Odermatt, et al. 2004. TCR affinity and negative regulation limit autoimmunity. *Nat. Med.* 10:1234–1239. http://dx.doi.org/10.1038/nm1114

Groom, J.R., J. Richmond, T.T. Murooka, E.W. Sorensen, J.H. Sung, K. Bankert, U.H. von Andrian, J.J. Moon, T.R. Mempel, and A.D. Luster. 2012. CXCR3 chemokine receptor-ligand interactions in the lymph node optimize CD4+ T helper 1 cell differentiation. *Immunity.* 37:1091–1103. http://dx.doi.org/10.1016/j.immuni.2012.08.016

Hancock, W.W., B. Lu, W. Gao, V. Csizmadia, K. Faia, J.A. King, S.T. Smiley, M. Ling, N.P. Gerard, and C. Gerard. 2000. Requirement of the chemokine receptor CXCR3 for acute allograft rejection. *J. Exp. Med.* 192:1515–1520. http://dx.doi.org/10.1084/jem.192.10.1515

Hardwick, L.J.A., and A. Philpott. 2014. Nervous decision-making: to divide or differentiate. *Trends Genet.* 30:254–261. http://dx.doi.org/10.1016/j.tig.2014.04.001

Henrickson, S.E., T.R. Mempel, I.B. Mazo, B. Liu, M.N. Artyomov, H. Zheng, A. Peixoto, M.P. Flynn, B. Senman, T. Junt, et al. 2008. T cell sensing of antigen dose governs interactive behavior with dendritic cells and sets a threshold for T cell activation. *Nat. Immunol.* 9:282–291. http://dx.doi.org/10.1038/ni1559

Henrickson, S.E., M. Perro, S.M. Loughhead, B. Senman, S. Stutte, M. Quigley, G. Alexe, M. Iannacone, M.P. Flynn, S. Omid, et al. 2013. Antigen availability determines CD8+ T cell-dendritic cell interaction kinetics and memory fate decisions. *Immunity.* 39:496–507. http://dx.doi.org/10.1016/j.immuni.2013.08.034

Hermans, I.F., D.S. Ritchie, J. Yang, J.M. Roberts, and F. Ronchese. 2000. CD8+ T cell-dependent elimination of dendritic cells in vivo limits the induction of antitumor immunity. *J. Immunol.* 164:3095–3101. http://dx.doi.org/10.4049/jimmunol.164.6.3095

Hickman, H.D., K. Takeda, C.N. Skon, F.R. Murray, S.E. Hensley, J. Loomis, G.N. Barber, J.R. Bennink, and J.W. Yewdell. 2008. Direct priming of antiviral CD8+ T cells in the peripheral interfollicular region of lymph nodes. *Nat. Immunol.* 9:155–165. http://dx.doi.org/10.1038/ni1557

Horwitz, M.S., Y. Yanagi, and M.B. Oldstone. 1994. T-cell receptors from virus-specific cytotoxic T lymphocytes recognizing a single immunodominant nine-amino-acid viral epitope show marked diversity. *J. Virol.* 68:352–357.

Hu, J.K., T. Kagari, J.M. Clingan, and M. Matloubian. 2011. Expression of chemokine receptor CXCR3 on T cells affects the balance between effector and memory CD8 T-cell generation. *Proc. Natl. Acad. Sci. USA.* 108:E118–E127. http://dx.doi.org/10.1073/pnas.1101881108

Huang, J., X. Zeng, N. Sigal, P.J. Lund, L.F. Su, H. Huang, Y.-H. Chien, and M.M. Davis. 2016. Detection, phenotyping, and quantification of antigen-specific T cells using a peptide-MHC dodecamer. *Proc. Natl. Acad. Sci. USA.* 113:E1890–E1897. http://dx.doi.org/10.1073/pnas.1602488113

Iezzi, G., K. Karjalainen, and A. Lanzavecchia. 1998. The duration of antigenic stimulation determines the fate of naive and effector T cells. *Immunity.* 8:89–95. http://dx.doi.org/10.1016/S1074-7613(00)80461-6

Kaech, S.M., and R. Ahmed. 2001. Memory CD8+ T cell differentiation: initial antigen encounter triggers a developmental program in naïve cells. *Nat. Immunol.* 2:415–422.

Kang, S.S., J. Herz, J.V. Kim, D. Nayak, P. Stewart-Hutchinson, M.L. Dustin, and D.B. McGavern. 2011. Migration of cytotoxic lymphocytes in cell cycle permits local MHC I–dependent control of division at sites of viral infection. *J. Exp. Med.* 208:747–759. http://dx.doi.org/10.1084/jem.20101295

Kastenmüller, W., P. Torabi-Parizi, N. Subramanian, T. Lämmermann, and R.N. Germain. 2012. A spatially-organized multicellular innate immune response in lymph nodes limits systemic pathogen spread. *Cell.* 150:1235–1248. http://dx.doi.org/10.1016/j.cell.2012.07.021

Kastenmüller, W., M. Brandes, Z. Wang, J. Herz, J.G. Egen, and R.N. Germain. 2013. Peripheral prepositioning and local CXCL9 chemokine-mediated guidance orchestrate rapid memory CD8+ T cell responses in the lymph node. *Immunity.* 38:502–513. http://dx.doi.org/10.1016/j.immuni.2012.11.012

Kearney, E.R., K.A. Pape, D.Y. Loh, and M.K. Jenkins. 1994. Visualization of peptide-specific T cell immunity and peripheral tolerance induction in vivo. *Immunity.* 1:327–339. http://dx.doi.org/10.1016/1074-7613(94)90084-1

Kitano, M., C. Yamazaki, A. Takumi, T. Ikeno, H. Hemmi, N. Takahashi, K. Shimizu, S.E. Fraser, K. Hoshino, T. Kaisho, and T. Okada. 2016. Imaging of the cross-presenting dendritic cell subsets in the skin-draining lymph node. *Proc. Natl. Acad. Sci. USA.* 113:1044–1049. http://dx.doi.org/10.1073/pnas.1513607113

Kohlmeier, J.E., W.W. Reiley, G. Perona-Wright, M.L. Freeman, E.J. Yager, L.M. Connor, E.L. Brincks, T. Cookenham, A.D. Roberts, C.E. Burkum, et al. 2011. Inflammatory chemokine receptors regulate CD8+ T cell contraction and memory generation following infection. *J. Exp. Med.* 208:1621–1634. http://dx.doi.org/10.1084/jem.20102110

Kurachi, M., J. Kurachi, F. Suenaga, T. Tsukui, J. Abe, S. Ueha, M. Tomura, K. Sugihara, S. Takamura, K. Kakimi, and K. Matsushima. 2011. Chemokine receptor CXCR3 facilitates CD8+ T cell differentiation into short-lived effector cells leading to memory degeneration. *J. Exp. Med.* 208:1605–1620. http://dx.doi.org/10.1084/jem.20102101

Kurachi, M., R.A. Barnitz, N. Yosef, P.M. Odorizzi, M.A. DiIorio, M.E. Lemieux, K. Yates, J. Godec, M.G. Klatt, A. Regev, et al. 2014. The transcription factor BATF operates as an essential differentiation checkpoint in early effector CD8+ T cells. *Nat. Immunol.* 15:373–383. http://dx.doi.org/10.1038/ni.2834

Ludewig, B., J.V. Stein, J. Sharpe, L. Cervantes-Barragan, V. Thiel, and G. Bocharov. 2012. A global "imaging" view on systems approaches in immunology. *Eur. J. Immunol.* 42:3116–3125. http://dx.doi.org/10.1002/eji.201242508

Man, K., M. Miasari, W. Shi, A. Xin, D.C. Henstridge, S. Preston, M. Pellegrini, G.T. Belz, G.K. Smyth, M.A. Febbraio, et al. 2013. The transcription factor IRF4 is essential for TCR affinity-mediated metabolic programming and clonal expansion of T cells. *Nat. Immunol.* 14:1155–1165. http://dx.doi.org/10.1038/ni.2710

Marchingo, J.M., A. Kan, R.M. Sutherland, K.R. Duffy, C.J. Wellard, G.T. Belz, A.M. Lew, M.R. Dowling, S. Heinzel, and P.D. Hodgkin. 2014. Antigen affinity, costimulation, and cytokine inputs sum linearly to

amplify T cell expansion. *Science.* 346:1123–1127. http://dx.doi.org/10.1126/science.1260044

Mempel, T.R., S.E. Henrickson, and U.H. Von Andrian. 2004. T-cell priming by dendritic cells in lymph nodes occurs in three distinct phases. *Nature.* 427:154–159. http://dx.doi.org/10.1038/nature02238

Moalli, F., J. Cupovic, F. Thelen, P. Halbherr, Y. Fukui, S. Narumiya, B. Ludewig, and J.V. Stein. 2014. Thromboxane A2 acts as tonic immunoregulator by preferential disruption of low-avidity $CD4^+$ T cell–dendritic cell interactions. *J. Exp. Med.* 211:2507–2517. http://dx.doi.org/10.1084/jem.20140137

Moreau, H.D., F. Lemaître, E. Terriac, G. Azar, M. Piel, A.-M. Lennon-Dumenil, and P. Bousso. 2012. Dynamic in situ cytometry uncovers T cell receptor signaling during immunological synapses and kinapses in vivo. *Immunity.* 37:351–363. http://dx.doi.org/10.1016/j.immuni.2012.05.014

Murphy, T.L., R. Tussiwand, and K.M. Murphy. 2013. Specificity through cooperation: BATF-IRF interactions control immune-regulatory networks. *Nat. Rev. Immunol.* 13:499–509. http://dx.doi.org/10.1038/nri3470

Nayar, R., E. Schutten, B. Bautista, K. Daniels, A.L. Prince, M. Enos, M.A. Brehm, S.L. Swain, R.M. Welsh, and L.J. Berg. 2014. Graded levels of IRF4 regulate $CD8^+$ T cell differentiation and expansion, but not attrition, in response to acute virus infection. *J. Immunol.* 192:5881–5893. http://dx.doi.org/10.4049/jimmunol.1303187

Newton, P., G. O'Boyle, Y. Jenkins, S. Ali, and J.A. Kirby. 2009. T cell extravasation: demonstration of synergy between activation of CXCR3 and the T cell receptor. *Mol. Immunol.* 47:485–492. http://dx.doi.org/10.1016/j.molimm.2009.08.021

Pace, L., A. Tempez, C. Arnold-Schrauf, F. Lemaitre, P. Bousso, L. Fetler, T. Sparwasser, and S. Amigorena. 2012. Regulatory T cells increase the avidity of primary $CD8^+$ T cell responses and promote memory. *Science.* 338:532–536. http://dx.doi.org/10.1126/science.1227049

Pham, T.H., T. Okada, M. Matloubian, C.G. Lo, and J.G. Cyster. 2008. $S1P_1$ receptor signaling overrides retention mediated by $G\alpha_i$-coupled receptors to promote T cell egress. *Immunity.* 28:122–133. http://dx.doi.org/10.1016/j.immuni.2007.11.017

Plumlee, C.R., B.S. Sheridan, B.B. Cicek, and L. Lefrançois. 2013. Environmental cues dictate the fate of individual $CD8^+$ T cells responding to infection. *Immunity.* 39:347–356. http://dx.doi.org/10.1016/j.immuni.2013.07.014

Preibisch, S., S. Saalfeld, and P. Tomancak. 2009. Globally optimal stitching of tiled 3D microscopic image acquisitions. *Bioinformatics.* 25:1463–1465. http://dx.doi.org/10.1093/bioinformatics/btp184

Preston, G.C., C. Feijoo-Carnero, N. Schurch, V.H. Cowling, and D.A. Cantrell. 2013. The impact of KLF2 modulation on the transcriptional program and function of CD8 T cells. *PLoS One.* 8:e77537. http://dx.doi.org/10.1371/journal.pone.0077537

Prlic, M., G. Hernandez-Hoyos, and M.J. Bevan. 2006. Duration of the initial TCR stimulus controls the magnitude but not functionality of the $CD8^+$ T cell response. *J. Exp. Med.* 203:2135–2143. http://dx.doi.org/10.1084/jem.20060928

Sabatino, J.J. Jr., J. Huang, C. Zhu, and B.D. Evavold. 2011. High prevalence of low affinity peptide–MHC II tetramer–negative effectors during polyclonal $CD4^+$ T cell responses. *J. Exp. Med.* 208:81–90. http://dx.doi.org/10.1084/jem.20101574

Savage, P.A., J.J. Boniface, and M.M. Davis. 1999. A kinetic basis for T cell receptor repertoire selection during an immune response. *Immunity.* 10:485–492. http://dx.doi.org/10.1016/S1074-7613(00)80048-5

Schumann, K., T. Lämmermann, M. Bruckner, D.F. Legler, J. Polleux, J.P. Spatz, G. Schuler, R. Förster, M.B. Lutz, L. Sorokin, and M. Sixt. 2010. Immobilized chemokine fields and soluble chemokine gradients cooperatively shape migration patterns of dendritic cells. *Immunity.* 32:703–713. http://dx.doi.org/10.1016/j.immuni.2010.04.017

Schwab, S.R., and J.G. Cyster. 2007. Finding a way out: lymphocyte egress from lymphoid organs. *Nat. Immunol.* 8:1295–1301. http://dx.doi.org/10.1038/ni1545

Slifka, M.K., and J.L. Whitton. 2001. Functional avidity maturation of $CD8^+$ T cells without selection of higher affinity TCR. *Nat. Immunol.* 2:711–717. http://dx.doi.org/10.1038/90650

Starbeck-Miller, G.R., H.-H. Xue, and J.T. Harty. 2014. IL-12 and type I interferon prolong the division of activated CD8 T cells by maintaining high-affinity IL-2 signaling in vivo. *J. Exp. Med.* 211:105–120. http://dx.doi.org/10.1084/jem.20130901

Sung, J.H., H. Zhang, E.A. Moseman, D. Alvarez, M. Iannacone, S.E. Henrickson, J.C. de la Torre, J.R. Groom, A.D. Luster, and U.H. von Andrian. 2012. Chemokine guidance of central memory T cells is critical for antiviral recall responses in lymph nodes. *Cell.* 150:1249–1263. http://dx.doi.org/10.1016/j.cell.2012.08.015

Susaki, E.A., K. Tainaka, D. Perrin, F. Kishino, T. Tawara, T.M. Watanabe, C. Yokoyama, H. Onoe, M. Eguchi, S. Yamaguchi, et al. 2014. Whole-brain imaging with single-cell resolution using chemical cocktails and computational analysis. *Cell.* 157:726–739. http://dx.doi.org/10.1016/j.cell.2014.03.042

Tkach, K., and G. Altan-Bonnet. 2013. T cell responses to antigen: hasty proposals resolved through long engagements. *Curr. Opin. Immunol.* 25:120–125. http://dx.doi.org/10.1016/j.coi.2012.12.001

Tomura, M., A. Hata, S. Matsuoka, F.H.W. Shand, Y. Nakanishi, R. Ikebuchi, S. Ueha, H. Tsutsui, K. Inaba, K. Matsushima, et al. 2014. Tracking and quantification of dendritic cell migration and antigen trafficking between the skin and lymph nodes. *Sci. Rep.* 4:6030. http://dx.doi.org/10.1038/srep06030

Turner, S.J., P.C. Doherty, J. McCluskey, and J. Rossjohn. 2006. Structural determinants of T-cell receptor bias in immunity. *Nat. Rev. Immunol.* 6:883–894. http://dx.doi.org/10.1038/nri1977

Ulvmar, M.H., K. Werth, A. Braun, P. Kelay, E. Hub, K. Eller, L. Chan, B. Lucas, I. Novitzky-Basso, K. Nakamura, et al. 2014. The atypical chemokine receptor CCRL1 shapes functional CCL21 gradients in lymph nodes. *Nat. Immunol.* 15:623–630. http://dx.doi.org/10.1038/ni.2889

van Gisbergen, K.P.J.M., P.L. Klarenbeek, N.A.M. Kragten, P.-P.A. Unger, M.B.B. Nieuwenhuis, F.M. Wensveen, A. ten Brinke, P.P. Tak, E. Eldering, M.A. Nolte, and R.A.W. van Lier. 2011. The costimulatory molecule CD27 maintains clonally diverse $CD8^+$ T cell responses of low antigen affinity to protect against viral variants. *Immunity.* 35:97–108. http://dx.doi.org/10.1016/j.immuni.2011.04.020

van Heijst, J.W.J., C. Gerlach, E. Swart, D. Sie, C. Nunes-Alves, R.M. Kerkhoven, R. Arens, M. Correia-Neves, K. Schepers, and T.N.M. Schumacher. 2009. Recruitment of antigen-specific $CD8^+$ T cells in response to infection is markedly efficient. *Science.* 325:1265–1269. http://dx.doi.org/10.1126/science.1175455

van Stipdonk, M.J., E.E. Lemmens, and S.P. Schoenberger. 2001. Naïve CTLs require a single brief period of antigenic stimulation for clonal expansion and differentiation. *Nat. Immunol.* 2:423–429.

van Stipdonk, M.J.B., G. Hardenberg, M.S. Bijker, E.E. Lemmens, N.M. Droin, D.R. Green, and S.P. Schoenberger. 2003. Dynamic programming of $CD8^+$ T lymphocyte responses. *Nat. Immunol.* 4:361–365. http://dx.doi.org/10.1038/ni912

Yao, S., B.F. Buzo, D. Pham, L. Jiang, E.J. Taparowsky, M.H. Kaplan, and J. Sun. 2013. Interferon regulatory factor 4 sustains $CD8^+$ T cell expansion and effector differentiation. *Immunity.* 39:833–845. http://dx.doi.org/10.1016/j.immuni.2013.10.007

Zehn, D., S.Y. Lee, and M.J. Bevan. 2009. Complete but curtailed T-cell response to very low-affinity antigen. *Nature.* 458:211–214. http://dx.doi.org/10.1038/nature07657